Observations and Morphology of the Cosmic Web

Rien van de Weygaert[1] and J. R. Bond[2]

[1] Kapteyn Astronomical Institute, University of Groningen, P.O. Box 800, 9700 AV Groningen, The Netherlands
weygaert@astro.rug.nl

[2] Canadian Institute for Theoretical Astrophysics, University of Toronto, TorontoWe describe here the essential properties and elements of the cosmic web as revealed in observations and simulations. ON M5S 1A7, Canada
bond@cita.utoronto.ca

1 Introduction

One of the most striking examples of a physical system displaying a salient geometrical morphology, and the largest in terms of sheer size, is the Universe as a whole. The past few decades have revealed that on scales of a few up to more than a hundred Megaparsec, the galaxies conglomerate into intriguing cellular or weblike patterns that pervade the observable cosmos.

The key structural components of the galaxy and cosmic mass distribution (see Fig. 1),

- Clusters
- Filaments
- Sheets/Walls
- Voids

are not merely randomly and independently scattered features. On the contrary, they have arranged themselves in a seemingly highly organized and structured fashion, the *Cosmic Foam* or *Cosmic Web*. They are woven into an intriguing *foamlike* tapestry that permeates the whole of the explored Universe. The vast under-populated *void* regions in the galaxy distribution represent both contrasting as well as complementary spatial components to the surrounding *planar* and *filamentary* density enhancements. At the intersections of the latter we often find the most prominent density enhancements in our universe, the rich *clusters* of galaxies (see Fig. 1).

In these notes we will delve into the observational and morphological aspects of the Cosmic Web. In the accompanying manuscript (van de Weygaert and Bond, [189]) we have presented the theory behind the emergence of the

R. Van de Weygaert and J. R. Bond: *Observations and Morphology of the Cosmic Web*, Lect. Notes Phys. **740**, 409–467 (2008)
DOI 10.1007/978-1-4020-6941-3_11

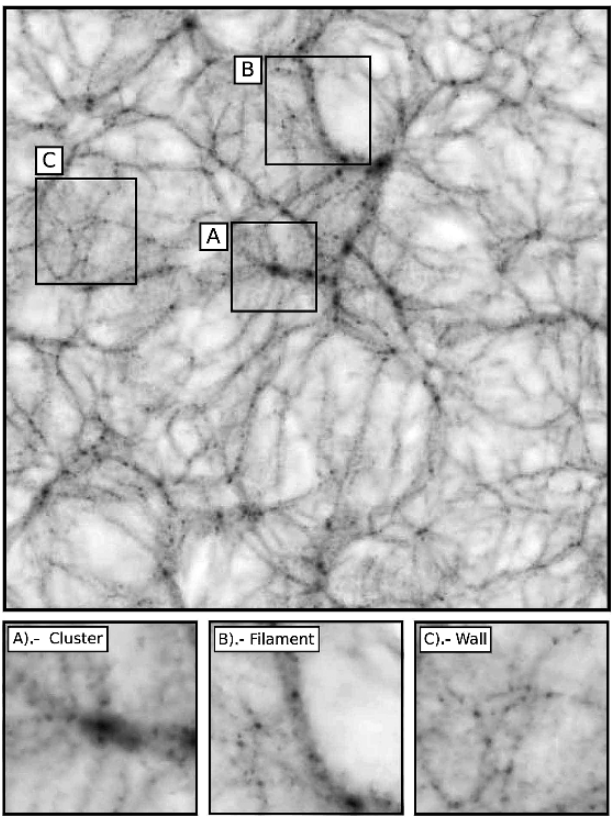

Fig. 1. The Cosmic Web. The image shows the weblike patterns traced by the Dark Matter distribution, at the present epoch, in a Universe based on a ΛCDM scenario. It concerns an N-body simulation in a box of $200\,h^{-1}$ Mpc size. The three boxes indicate examples of the main structure components of the Cosmic Web. Amongst others, the image clarifies the mutual spatial relationship between these elements. Low-density and low contrast walls are less prominent than the outstanding filamentary channels which define the texture of the Cosmic Web. Near the intersection points of filaments and sheets we find high-density cluster nodes. The figures demonstrates the significance of the concept "Cosmic Web". Image courtesy of Miguel Aragón-Calvo, see Aragón-Calvo [5]

Cosmic Web from the pristine near-uniform Universe. The theoretical framework of *Cosmic Web* has to be confronted with the information obtained from a variety of sources. On the observational side the cosmic web has first been seen in redshift maps of the spatial galaxy distribution. The recent success in mapping the spatial weblike dark matter distribution by means of weak lensing observations forms a breakthrough for our understanding of the large-scale dynamics. Equally important sources of information concern the Lyα forest and the WHIM, the imprint of the gaseous material that fell into the weblike

structures defined by the dark matter distribution. Two aspects of the large scale universe do play a special role in our study. Clusters of galaxies are the prime objects in defining the pattern and structure of the Cosmic Web. On the other hand we have the large voids as important structural and dynamical components. They are of prime significance for the morphology of the large scale Universe.

2 The Emergence of the Cosmic Web

Towards the end of the seventies a set of new observations did start to unveil the existence of coherent structures larger than that of clusters of galaxies. With the review of [124] the supercluster paradigm established itself as the new view of the large scale distribution of matter and galaxies in the Universe. It had gradually emerged as a result of various early galaxy redshift surveys of nearby regions in the Universe (e.g. Chincarini and Rood [33], Gregory and Thompson [73], Einssto, Joeveer and Saar [55]) and put on a firm fotting with the completion of the first systematic and large redshift survye, the CfA1 survey [43]. Along with these efforts came the unexpected finding of the first example of large cosmic voids, the Bootes void [96].

2.1 Galaxies and the Cosmic Web

It was the celebrated map of the first CfA redshift slice [45] that showed the connection between the basic elements of the Cosmic Web that was going to emerge in the more complete picture. While it provided an initial hint of the existence of the Cosmic Web it was so thin that it was not immediately clear what its true nature was, whether it were bubbles, pancakes, or something else. In recent years this view has been expanded dramatically to the present grand vistas offered by the 100,000s of galaxies in the 2dF – two-degree field – Galaxy Redshift Survey, the 2dFGRS (e.g. Colless et al. [39]), and SDSS [180] galaxy redshift surveys.[1] These and many other redshift surveys have unequivocally established that galaxies are located in dense, compact clusters, in less dense filaments, and in sheetlike walls surrounding vast, almost empty regions called voids, the structural components of the Cosmic Web.

The first impressions of a weblike galaxy distribution seen in the shallow CfA2 redshift slices got firmly established as a universal cosmic phenomenon through the publication of the results of the Las Campanas redshift survey (LCRS [166]). Its chart of 26,000 galaxy locations in six thin strips on the sky, extending out to a redshift of $z \sim 0.1$, did provide the first impression of structure in a truely cosmologically representative volume of space. The Las Campanas redshift survey confirmed the ubiquity and reality of weblike patterns over vast reaches of our Universe. Also important was that it did not show any strong evidence of inhomogeneities surpassing sizes of $100 - 200\,\mathrm{h}^{-1}\mathrm{Mpc}$.

[1] See `http://www.mso.anu.edu.au/2dFGRS/` and `http://www.sdss.org/`

This is most dramatically illustrated by the map 2dFGRS and SDSS maps. The published maps of the distribution of nearly 250,000 galaxies in two narrow "slice" regions on the sky yielded by the 2dFGRS surveys reveal a far from homogeneous distribution. Instead, we recognize a sponge-like arrangement, with galaxies aggregating in striking geometric patterns such as prominent filaments, vaguely detectable walls and dense compact clusters on the periphery of giant voids.[2] The three-dimensional view emerging from the SDSS redshift survey provides an even more convincing image of the intricate patterns defined by the cosmic web (Fig. 2). A careful assessment of the galaxy distribution in our immediate vicintiy reveals us how we ourselves are embedded and surrounded by beautifully delineated and surprisingly sharply defined weblike structures. In particular the all-sky nearby infrared 2MASS survey (see Fig. 3) provides us with a meticulously clear view of the web surrounding us.

The cosmic web is outlined by galaxies populating huge *filamentary* and *wall-like* structures, the sizes of the most conspicuous one frequently exceeding $100\,\mathrm{h}^{-1}$ Mpc. The closest and best studied of these massive anisotropic matter concentrations can be identified with known supercluster complexes, enormous structures comprising one or more rich clusters of galaxies and a plethora of more modestly sized clumps of galaxies. A prominent and representative nearby specimen is the Perseus-Pisces supercluster, a $5\,\mathrm{h}^{-1}$ wide ridge of at least $50\,\mathrm{h}^{-1}$ Mpc length, possibly extending out to a total length of $140\,\mathrm{h}^{-1}$ Mpc. While such giant elongated structures are amongst the most conspicuous features of the Megaparsec matter distribution, filamentary features are encountered over a range of scales and seem to represent a ubiquitous and universal state of concentration of matter. In addition to the presence of such filaments the galaxy distribution also contains vast planar assemblies. A striking local example is the *Great Wall*, a huge planar concentration of galaxies with dimensions that are estimated to be of the order of $60\,\mathrm{h}^{-1} \times 170\,\mathrm{h}^{-1} \times 5\,\mathrm{h}^{-1}$ Mpc [66]. In both the SDSS and 2dF surveys even more impressive planar complexes were recognized, with dimensions substantially in excess of those of the local Great Wall. At the moment, the socalled *SDSS Great Wall* appears to be the largest known structure in the Universe (see Fig. 4).

2.2 Cosmic Nodes: Clusters

Within and around these anisotropic features we find a variety of density condensations, ranging from modest groups of a few galaxies up to massive compact *galaxy clusters* (see eg. Fig. 5). The latter stand out as the most massive, and most recently, fully collapsed and virialized objects in the Universe.

[2] It is important to realize that the interpretation of the Megaparsec galaxy distribution is based upon the tacit yet common assumption that it forms a a fair reflection of the underlying matter distribution. While there are various indications that this is indeed a reasonable approximation, as long as the intricate and complex process of the formation of galaxies has not been properly understood this should be considered as a plausible yet heuristic working hypothesis.

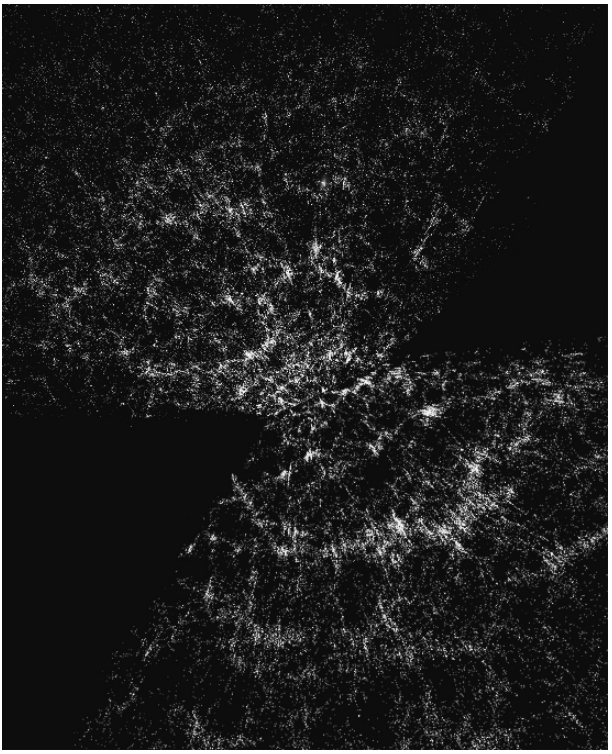

Fig. 2. SDSS is the largest and most systematic sky survey in the history of astronomy. It is a combination of a sky survey in 5 optical bands of 25% of the celestial (northern) sphere. Each image is recorded on CCDs in these 5 bands. On the basis of the images/colours and their brightness a million galaxies are subsequently selected for spectroscopic follow-up. The total sky area covered by SDSS is 8452 square degrees. Objects will be recorded to $m_{\rm lim} = 23.1$. In total the resulting atlas will contain 10^8 stars, 10^8 galaxies and 10^5 quasars. Spectra are taken of around 10^6 galaxies, 10^5 quasars and 10^5 unusual stars (in our Galaxy). Of the 5 public data releases 4 have been accomplished, ie. 6670 square degrees of images is publicly available, along with 806,400 spectra. In total, the sky survey is now completely done (107%), the spectroscopic survey for 68%. This image is taken from a movie made by Subbarao, Surendran and Landsberg (see website: http://astro.uchicago.edu/cosmus/projects/sloangalaxies/). It depicts the resulting redshift distribution after the 3rd public data release. It concerns 5282 square degrees and contained 528,640 spectra, of which 374,767 galaxies

Approximately 4% of the mass in the Universe is assembled in rich clusters. They may be regarded as a particular population of cosmic structure beacons as they typically concentrate near the interstices of the cosmic web, *nodes* forming a recognizable tracer of the cosmic matter distribution [23]. Clusters not only function as wonderful tracers of structure over scales of dozens up to

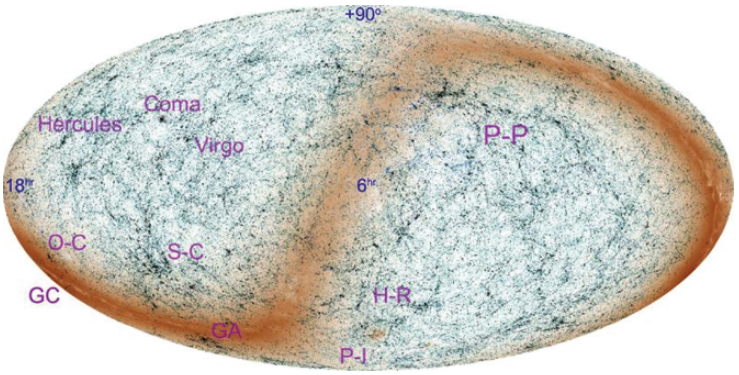

Fig. 3. Equatorial view of the 2MASS galaxy catalog (6h RA at centre). The grey-scale represents the total integrated flux along the line of sight – the nearest (and therefore brightest) galaxies produce a vivid contrast between the Local Supercluster (**centre-left**) and the more distant cosmic web. The dark band of the Milky Way clearly demonstrates where the galaxy catalog becomes incomplete due to source confusion. Some well known large-scale structures are indicated: P-P=Perseus-Pisces supercluster; H-R=Horologium-Reticulum supercluster; P-I=Pavo-Indus supercluster; GA='Great Attractor'; GC=Galactic Centre; S-C=Shapley Concentration; O-C=Ophiuchus Cluster; Virgo, Coma, and Hercules=Virgo, Coma and Hercules superclusters. The Galactic 'anti-centre' is front and centre, with the Orion and Taurus Giant Molecular Clouds forming the dark circular band near the centre. Image courtesy of J.H. Jarrett. Reproduced with permission from the Publications of the Astronomical Society of Australia 21(4): 396–403 (T.H. Jarrett). Copyright Astronomical Society of Australia 2004. Published by CSIRO PUBLISHING, Melbourne Australia

hundred of Megaparsec but also as useful probes for precision cosmology on the basis of their unique physical properties.

The richest clusters contain many thousands of galaxies within a relatively small volume of only a few Megaparsec size. For instance, in the nearby Virgo and Coma clusters more than a thousand galaxies have been identified within a radius of a mere $1.5\,\mathrm{h}^{-1}$ Mpc around their core (see Fig. 6). Clusters are first and foremost dense concentrations of dark matter, representing overdensities $\Delta \sim 1000$. In a sense galaxies and stars only form a minor constituent of clusters. The cluster galaxies are trapped and embedded in the deep gravitational wells of the dark matter. These are identified as a major source of X-ray emission, emerging from the diffuse extremely hot gas trapped in them. While it fell into the potential well, the gas got shock-heated to temperatures in excess of $T > 10^7$ K, which results in intense X-ray emission due to the bremsstrahlung radiated by the electrons in the highly ionized intracluster gas. In a sense clusters may be seen as hot balls of X-ray radiating gas. The amount of intracluster gas in the cluster is comparable to that locked into

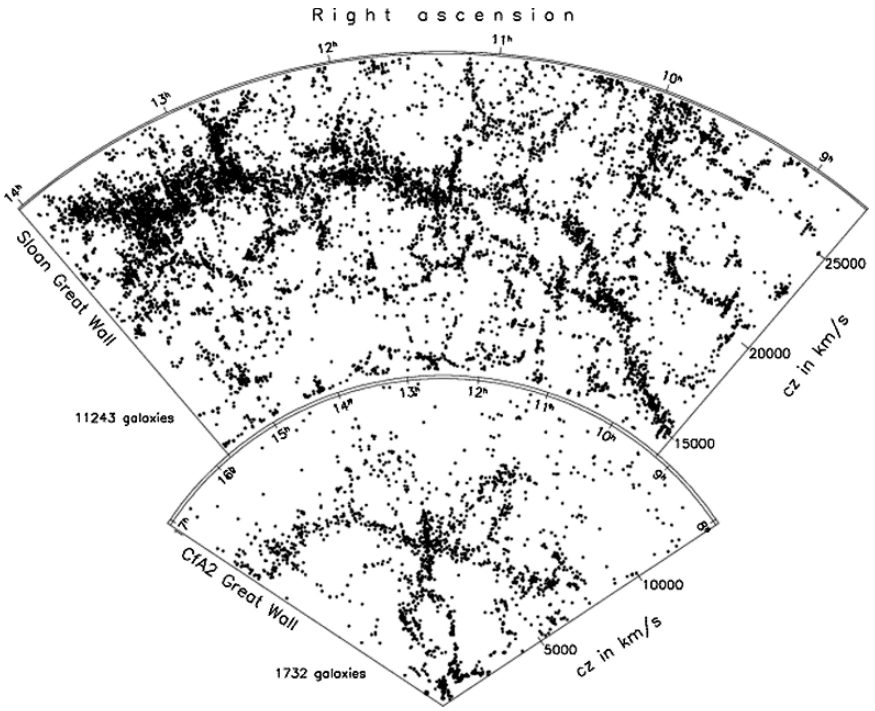

Fig. 4. The CfA Great Wall (bottom slice, Geller and Huchra [66]) compared with the Sloan Great Wall (**top slice**). Both structures represent the largest coherent structural in the galaxy redshift surveys in which they were detected, the CfA redshift survey and the SDSS redshift survey. The (CfA) Great Wall is a huge planar concentration of galaxies with dimensions that are estimated to be of the order of $60\,\mathrm{h}^{-1} \times 170\,\mathrm{h}^{-1} \times 5\,\mathrm{h}^{-1}$ Mpc. Truely mindboggling is the Sloan Great Wall, a huge conglomerate of clusters and galaxies. With a size in the order of $400\ \mathrm{h}^{-1}$ Mpc it is at least three times larger than the CfA Great Wall. It remains to be seen whether it is a genuine physical structure or mainly a stochastic arrangement and enhancement, at a distance coinciding with the survey's maximum in the radial selection function. Image courtesy of M. Jurić, see also Gott et al. [70]. Reproduced by permission of the AAS

stars, and stands for $\Omega_{\mathrm{ICM}} \sim 0.0018$ [63]. The X-ray emission represents a particularly useful signature, an objective and clean measure of the potential well depth, directly related to the total mass of the cluster (see e.g. Reiprich and Böhringer, [146]). Through their X-ray brightness they can be seen out to large cosmic depths. The deep gravitational dark matter wells also strongly affects the path of passing photons. While the resulting strong lensing arcs form a spectacular manifestation, it has been the more moderate distortion of background galaxy images in the weak lensing regime [88, 89] which has opened up a new window onto the Universe. The latter has provided a direct

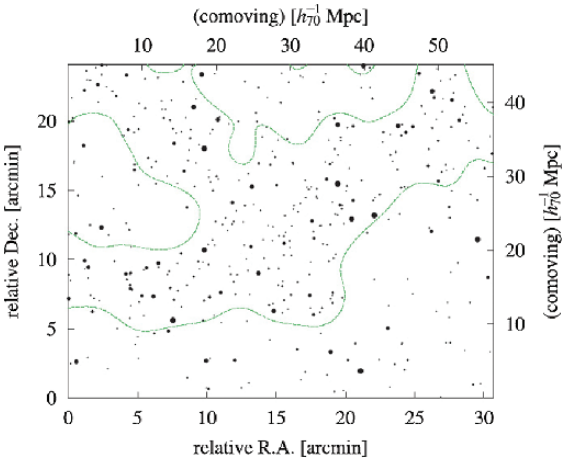

Fig. 5. The cosmic web at high redshifts: a prominent weblike features at a redshift $z \sim 3.1$ found in a deep view obtained by the Subaru telescope. Large scale sky distribution of 283 strong Lyα emitters (*black filled circles*), the Lyα absorbers (*red filled circles*) and the extended Lyα emitters (*blue open squares*). The dashed lines indicate the high-density region of the strong Lyα emitters. From Hayashino et al. 2004. Reproduced by permission of the AAS

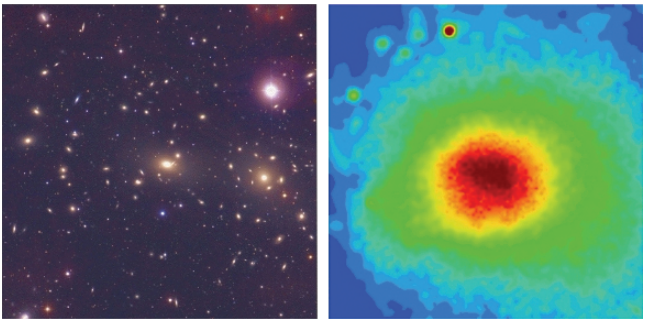

Fig. 6. Comparison of optical and X-ray images of the Coma cluster, A1656. The cluster is at a distance of $\approx 70\,\mathrm{h}^{-1}$ Mpc. **Left:** optical image of the galaxies in the centre of the Coma cluster. The Coma cluster contains more than 1000 galaxies within a central region of $\approx 1.5\,\mathrm{h}^{-1}$ Mpc, mostly elliptical and SO galaxies. Clearly visible are the two dominant giant elliptical galaxies, NGC4878 and NGC4889. The colour image was created from 3 separate exposures taken in blue, red and near-infrared, with the KPNO 0.9 m telescope (courtesy of Omar López-Cruz). **Right:** ROSAT X-ray image at 0.5–2.0 keV.of the central region of the Coma cluster (courtesy: S.L. Snowden, NASA/GSFC). The image is $\approx 1^\circ \times 1^\circ$, corresponding to a size of $1.2\,\mathrm{h}^{-1}$ Mpc at the cluster's redshift $z = 0.0232$

probe of the dark matter content of clusters and the large scale universe (for a review see e.g. Mellier [118], Refregier [144]) (also see Sect. 2.4).

Cluster Catalogs

The Abell catalogue of optically identified galaxy clusters [2, 3] has fulfilled a central role for the study of clusters and their large scale matter distribution on scales of several tens of Megaparsec (see Bahcall [9]). With the arrival of large new galaxy redshift surveys deep and objectively identified cluster samples have opened a plethora of elaborate, detailed and systematic studies of the cluster population. Cluster samples extracted from the SDSS survey [15, 119, 150] will continue to play a large role. New and objective cluster detection techniques have improved the range and completeness of the cluster samples while minimizing projection effects [67, 95, 119]. Projection effects may evoke false detections and contaminate studies of the cluster large scale distribution. Amongst the most promising methods for optical or NIR cluster detection is that of *red-sequence detection* [67], in which clusters are simultaneously detected as overdensities in projected angular position, colour and magnitude. It uses the observational fact that the bulk of the early-type galaxies in rich clusters lie along a linear and narrow colour-magnitude relation [109, 196]. The Red-Sequence Cluster Survey (RCS) seeks to exploit this observation to compose a large catalog of clusters. Extrapolating cluster detection towards the NIR, Kochanek et al. [100] assembled a cluster catalog from the 2MASS galaxy sample. Other cluster samples are selected through their X-ray emission, believed to represent a more robust manner for selecting mass-limited samples. Particularly noteworthy is the ROSAT-ESO Flux Limited X-ray catalog (REFLEX [21]), which contains all clusters brighter than an X-ray flux of 3×10^{-12} ergs^{-1} cm^{-2} over a large part of the southern sky. In addition there is the RASS X-ray selected SDSS cluster sample [141], combining both optical and X-ray selection criteria. Recently, within the context of the Deep Lens Survey, Wittman et al. [195] presented the first cluster sample on the basis of their weak gravitational lensing signature. Perhaps potentially most promising is the use of the Sunyaev-Zel'dovich effect, the small CMB spectral distortion caused by the scattering of the CMB photons off the high-energy intracluster electrons [175, 176]. Carlstrom et al. [28] and Vale and White [185] proposed the construction of cluster catalogs using the SZ effect. While the Planck satellite mission will certainly be a major step forward in the detection of SZ clusters, optimism has been slightly tempered by the recent result of Lieu et al. [104]. Within the WMAP observations centered on 31 clusters they found a CDM decrement which was at least a factor 4 smaller than expected.

Cluster Clustering

Through their high visibility clusters can be traced out to vast distances in the Universe. Following the basic assumption that they are a fair and direct, be it

sparse, tracer of the underlying matter distribution clusters are ideally suited for probing the spatial matter distribution over large regions of space. Maps of their distribution contain information on spatial clustering on scales of up to hundreds of Megaparsec. A large range of observational studies, mostly based on optically or X-ray selected samples, display a substantial level of clumping of clusters on scales where clustering in the galaxy distribution has diminished below detectability levels. A wide range of observational studies on the basis of such optically selected samples have shown that the clustering of clusters is significantly more pronounced than that of galaxies. Their two-point correlation function has a shape similar to that of galaxies, but with a substantially higher amplitude and detectable out to distances of at least $\sim 50\ \ h^{-1}$ Mpc.

A good impression of the spatial distribution of rich clusters may be obtained from Fig. 7 (from Borgani and Guzzo, [23]). It shows the spatial distribution of the clusters in the REFLEX galaxy cluster catalogue [21]. Maps such as these confirm that clusters are highly clustered [9, 23]. They aggregate to form huge supercluster complexes, coinciding with the filaments, walls and related features in the galaxy distribution. These superclusters are

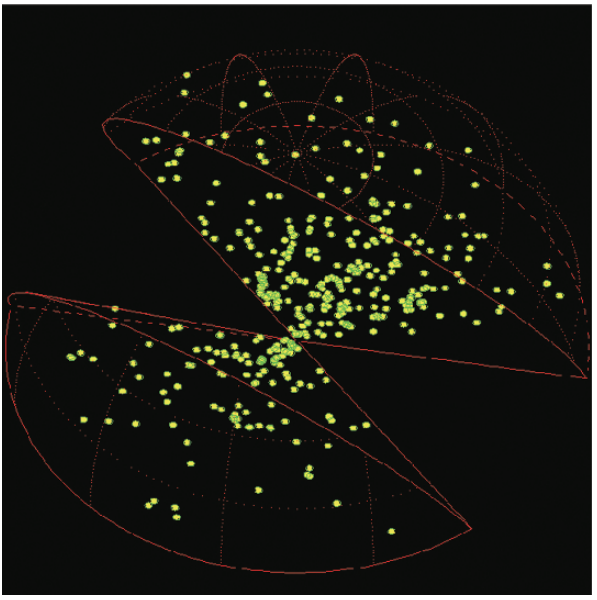

Fig. 7. The spatial cluster distribution. The full volume of the X-ray REFLEX cluster survey within a distance of $600\,h^{-1}$Mpc. The REFLEX galaxy cluster catalogue [21], contains all clusters brighter than an X-ray flux of $3 \times 10^{-12}\,\mathrm{ergs}^{-1}\mathrm{cm}^{-2}$ over a large part of the southern sky. The missing part of the hemisphere delineates the region highly obscured by the Galaxy. Courtesy: Borgani and Guzzo [23]. Reproduced by permission of Nature

moderate density enhancements on scale of tens of Megaparsec, typically in the order of a few times the average density. Either they are still co-expanding with the Hubble flow, be it at a slightly decelerated rate, or they just started contracting. Within these structures clusters reside at the dense intersections of filaments, along which mass drains into the massive clusters [190].

Cluster Dipole

Clusters may also provide a better and more extensive view of the contributions to the local gravitational force field by comparing the inferred Local Group motion to the CMB dipole. Scaramella et al. [159] and Plionis and Valdarnini [137] sought to establish by means of the cluster distribution within a distance of $r \approx 300$ h^{-1}Mpc whether the origin of our cosmic motion should be located within this volume, or whether there are indications for even larger cosmic structures. Interestingly, the results of Plionis & Kolokotronis [138] and Kocevski and Ebeling [99] appears to suggest that X-ray selected clusters in the nearby Universe indicate a significantly larger dynamical influence of structures over scales of 150 h^{-1} Mpc than previously indicated by similar dipole studies on the basis of the IRAS Point Source Catalog Redshift survey (PSCz, see e.g. Branchini et al. [26]) and the dipole anisotropy of the 2MASS Redshift survey [59]. The latter find that mass structures beyond a distance of 140 h^{-1} Mpc only induce a negligible acceleration on the Local Group. Using the combined X-ray REFLEX, eBCS [54] and CIZA samples, [99] came to the conclusion that only 44% of the local motion is due to infall into the Great Attractor region while 56% is induced by more distant mass concentrations between 130 h^{-1} Mpc and 180 h^{-1} Mpc away. The Shapley supercluster, one of the largest concentrations of clusters out to $z = 0.12$, is responsible for at least 30% of the acceleration induced by structures beyond 130 h^{-1} Mpc. Also the Horologium-Reticulum supercluster is found to have a substantial impact. The schematic dipole profile (Fig. 8) indeed provides an enticing insight into the implied local cosmic dynamics. Also interesting is the presence of a significant underdensity in the cluster distribution on the nother hemisphere, at a distance ~ 150 h^{-1} Mpc.

Cluster Bias

The results on the strong clustering of clusters motivated theoretical arguments for the idea of them forming a biased tracer of the matter distribution. The first simple linear biasing prescriptions were justified by the idea that clusters form from high-density peaks in the primordial density field, filtered over an appropriately large scale [10, 87]. Biasing prescriptions may incorporate or quantify an array of complex and usually ununderstood *"gastrophysical"* processes [49]. However, to understand the influence on clustering it may suffice to derive a heuristic bias factor of function. The value of a simple (linear) *bias*

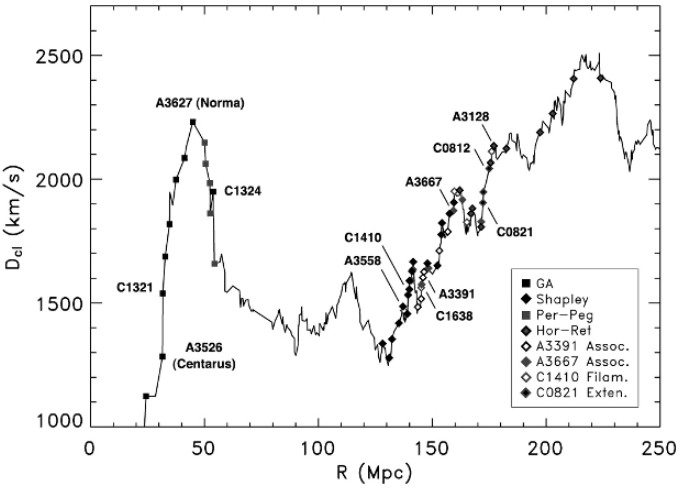

Fig. 8. Schematic X-ray cluster dipole profile. Clusters associations are grouped by symbol shading to highlight their impact on the overall dipole amplitude. Abell and CIZA clusters begin with letters "A" and "C". Acronyms are: GA/Great Attractor, Hor-Ret/Horologium-Reticulum, Per-Peg/Perseus-Pegasus. Image courtesy: Kocevski and Ebeling [99]. Reproduced by permission of AAS

factor would be a function of cluster mass, structure formation scenario and cosmic epoch. Following up on the original *peak bias* idea [10, 87], an array of more sophisticated theoretical bias model have been proposed. Seeking to describe and analyze the bias of different species of galaxies as well as of clusters, these modifications elaborated upon this idea and increased the realism of the approximation [13, 48, 115, 120, 179].

2.3 Cosmic Depressions: the Voids

Complementing this cosmic inventory leads to the existence of large *voids*, enormous regions with sizes in the range of 20–50 h^{-1} Mpc that are practically devoid of any galaxy, usually roundish in shape and occupying the major share of space in the Universe. Forming an essential ingredient of the *Cosmic Web*, they are surrounded by elongated filaments, sheetlike walls and dense compact clusters.

Voids have been known as a feature of galaxy surveys since the first surveys were compiled [33, 55, 73]. Following the discovery by Kirshner et al. [96, 97] of the most dramatic specimen, the Boötes void, a hint of their central position within a weblike arrangement came with the first CfA redshift slice [45]. This view has been dramatically endorsed and expanded by the redshift maps of the 2dFGRS and SDSS surveys [1, 39]. They have established voids as an integral component of the Cosmic Web. The 2dFGRS maps and SDSS maps (see e.g. Figs. 2 and 10), and the void map of the 6dF survey in Fig. 9, are

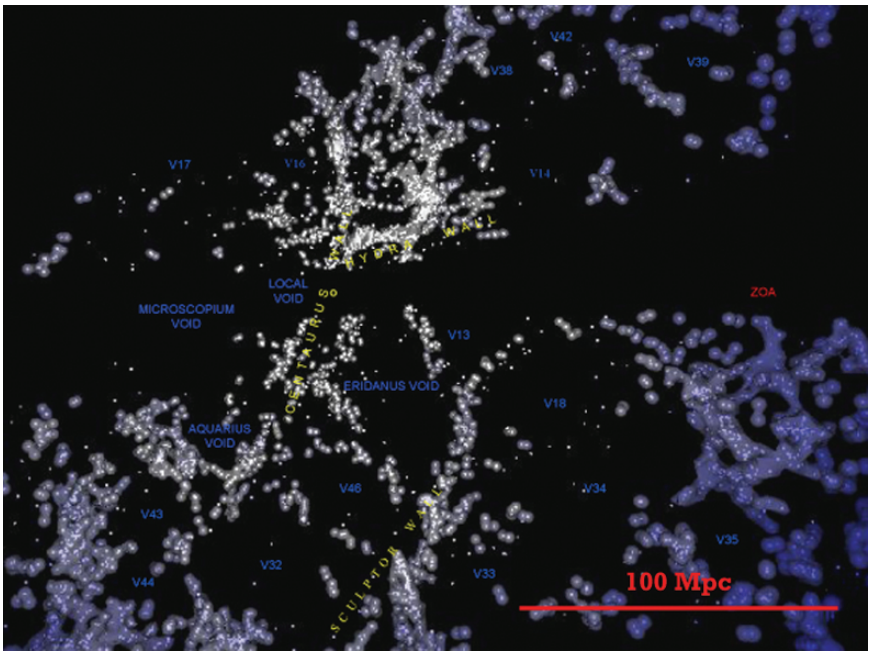

Fig. 9. A region of the 6dF redshift survey marked by the presence of various major voids. The image concerns a 3D rendering of the galaxy distribution in a 1000 km/s thick slice along the supergalactic SGX direction, at SGX = −2500 km/s. Image courtesy of A. Fairall

telling illustrations of the ubiquity and prominence of voids in the cosmic galaxy distribution.

For the most systematic and complete impression of the cosmic void population the Local Universe provides the most accessible region. Recently, the deep view of the 2dFGRS and SDSS probes (see e.g. Fig. 12) has been supplemented with high-resolution studies of voids in the nearby Universe. Based upon the 6dF survey [77], Fairall (private communication) identified nearly all voids within the surveyed region out to 35,000 km s^{-1}. It is the 2MASS redshift survey [83] – the densest all-sky redshift survey available – which has provided a uniquely detailed census of large scale structures in our Local Universe [59]. Partially including 6dF redshifts, the 2MASS redshift survey entails a complete and systematic survey of structure in the nearby Universe up to 14,000–16,000 km s^{-1}. This includes a complete sample of voids, directly identifiable from the density and velocity field reconstruction by Erdoğdu et al. [59] does contain a nice complete sample of voids in our Local Universe, although though some measure of bias and upper-limit to the size of identifiable voids is introduced via the substantial level of spatial smoothing going along with the Wiener filter processing. A nice impression of the typical structure, geometry and size of voids is given by shell section through the local Cosmic Web seen in the Aitoff sky projection in Fig. 11.

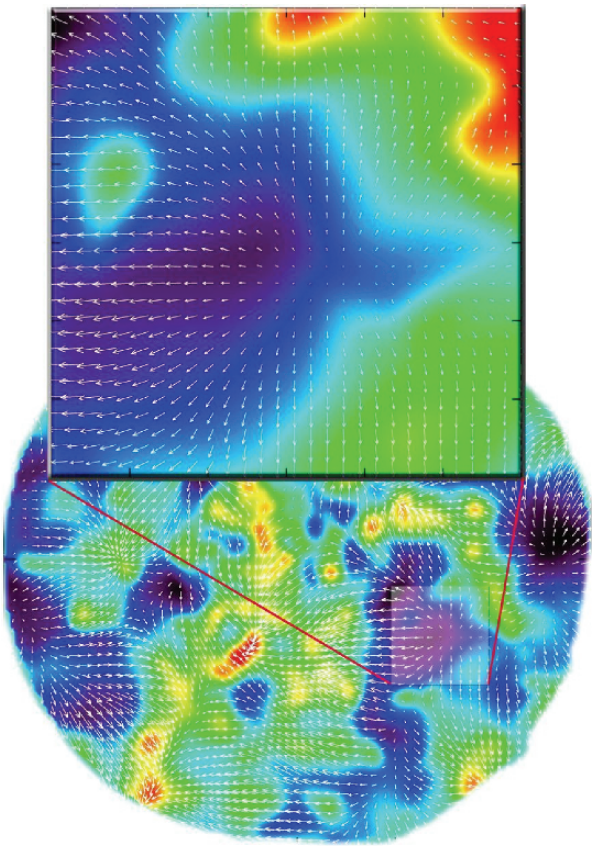

Fig. 10. Gravitational impact of the Sculptor Void. The righthand frame shows the inferred velocity field in and around the Sculptor void near the Local Supercluster. The colour map represents the density values, with dark blue at $\delta \sim -0.75$ and cyan near $\delta \sim 0.0$. The vectors show the implied velocity flow around the void, with a distinct nearly spherically symmetric outflow. It is a zoom-in onto the indicated region in the density and velocity map in the Local Universe (lefthand) determined on the basis of the PSCz galaxy redshift survey. The peculiar velocities of the galaxies in the PSCz galaxy redshift catalogue were determined by means of a linearization procedure [25], the resulting galaxy positions and velocities have been translated by DTFE into the depicted density and velocity flow maps. The Local Group is at the centre of the map of our Local Universe (lefthand). To the left we see the Great Attractor region extending out towards the Shapley supercluster. To the righthand side we can find the Pisces-Perseus supercluster. The density values range from ~ 4.9 (red) down to ~ -0.75 (darkblue), with cyan coloured regions having a density near the global cosmic average ($\delta \sim 0$). The velocity vectors are scaled such that a vector with a length of $\approx 1/33$rd of the region's diameter corresponds to 650 km/s. The density and velocity field have an effective Gaussian smoothing radius of $R_G \sim \sqrt{5}\ \mathrm{h}^{-1}$ Mpc. The top righthand insert zooms in on the Local Supercluster and Great Attractor complex. From: Romano-Díaz and van de Weygaert [149]

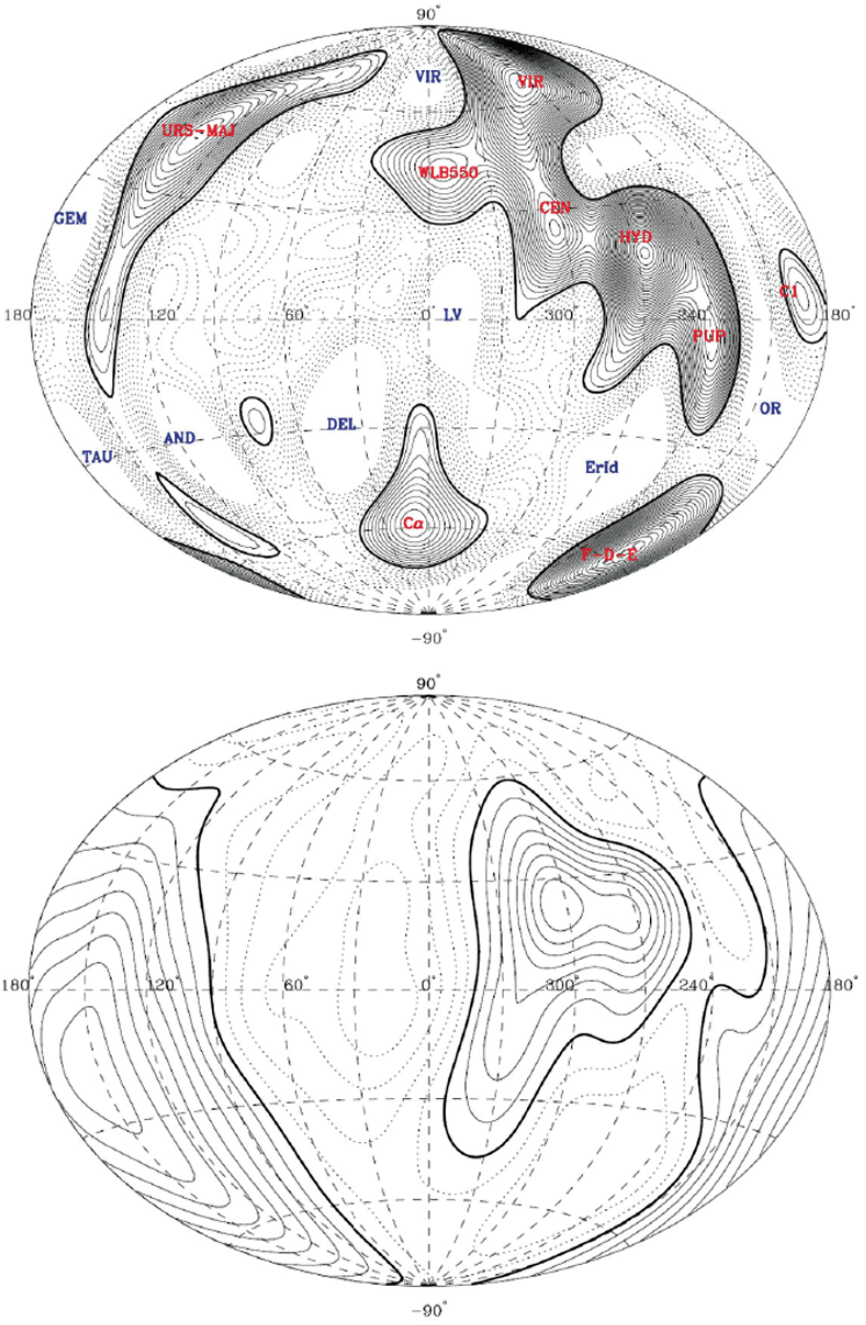

Fig. 11. (continued)

Void Sizes

Voids in the galaxy distribution account for about 95% of the total volume (see Kauffmann and Fairall [93], El-Ad, Piran and da Casta [56], El-Ad and Piran [57], Hoyle and Vogeley [81], Plionis and Basilakos [139], Rojas et al. [148], Platen, van de Weygaert and Jones [137]).

The typical sizes of voids in the galaxy distribution depend on the galaxy population used to define the voids. Voids defined by galaxies brighter than a typical L_* galaxy tend to have diameters of order 10–20 h^{-1}Mpc, but voids associated with rare luminous galaxies can be considerably larger; diameters in the range of 20–50 h^{-1} Mpc are not uncommon (e.g Hoyle and Vogeley [81], Plionis and Basilakos [139]). These large sizes mean that only now we are beginning to probe a sufficiently large cosmological volume to allow meaningful statistics with voids to be done. Firm upper limits on the maximum void size have not yet been set. Recently there have been claims of the existence of a supersized void, in the counts of the NVVS catalogue of radio sourcs, and of its possible imprint on the CMB via the ISW effect in the form of a 'cold spot'. If this will be confirmed it will pose an interesting challenge to any cosmological scenario (see Rudnick et al. [151]).

At the low end side of the void size distribution a very detailed survey of the Local Volume, the very nearby Universe in and immediately around our Local Supercluster, does provide some tentative information. At this close range a few studies claim to have found what may be the smallest genuine voids in existence. In his Catalog and Atlas of Nearby Galaxies Tully [183] noted the presence of the *Local Void* in the Local Supercluster. The Local Void begins directly from the boundaries of the Local Group and extends in the direction of the north pole of the LSC by $\sim$ 14 h^{-1} Mpc. Similar and even smaller minivoids have recently been found by the analysis of Tikhonov and Karachentsev [181] of the galaxy distribution in the Catalog of

Fig. 11. (continued) 2MASS view of the Local Void outflow. The reconstructed density (**top frame**) and velocity field (**bottom frame**) of the 2MASS redshift survey, evaluated on a thin shell of 2000 km s^{-1}, shown in Aitoff projection. From Erdoğdu et al. [59]. Top: the reconstructed density field in the thin shell, providing a telling section through the Local Cosmic Web. Dashed lines show $\delta < 0$, solid lines $\delta \geq 0$, with contour spacing of $\Delta\delta = 0.1$. Easily identifiable overdensities are Ura Major, the Virgo cluster, the Centaurus cluster, Hydra cluster and the Fornax-Doradus-Eridanus (F-D-E) supercluster complex. Most interestingly are the locations of local voids: Gemini (Gem), Taurus (Tau), Andromeda (And), Delphinus (Del), Virgo (Vir), Eridanus (Erid), Orion (Ori), and the Local Void (LV). Bottom: Dashed lines show infall velocities, solid lines outflow. First solid line is for $v_{\rm rad} = 0$ km s^{-1}, and contour spacing is $|\Delta v_{\rm rad}| = 50$ km s^{-1}. Clearly visible is the strong outflow from the Local Void, reflected in the strong central patch. From: Erdoğdu et al. [59]

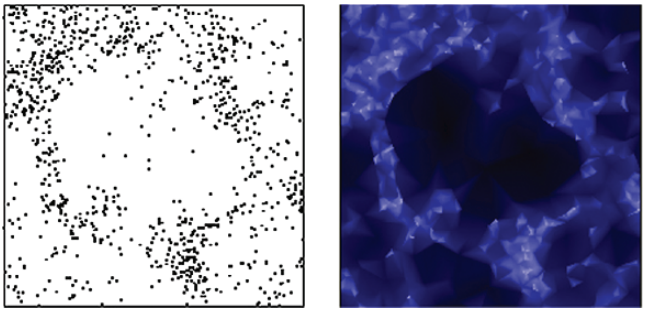

Fig. 12. Void region in de 2dFGRS survey. From: Schaap [160]

Neighbouring Galaxies [92]. Because the latter entails a meticulously detailed view of the true spatial distribution of galaxies out to 5 h^{-1} Mpc, it allowed the identification and mapping of minivoids in the Local Volume. Tikhonov and Karachentsev [181] and Tikhonov and Klypin [182] claim to have found a total of some 30 minivoids, completely free of galaxies, with sizes of 0.7–3.5 h^{-1} Mpc.

The Meaning of Voids

There are a variety of reasons why the study of voids is interesting for our understanding of the cosmos.

- Firstly, because they are a prominent aspect of the Megaparsec Universe it is necessary to understand the structure of evolution of voids in order to get a proper and full understanding of the formation and dynamics of the Cosmic Web.
- Secondly, voids may contain a considerable amount of information on the underlying cosmological scenario and on global cosmological parameters.
- Thirdly, their pristine low-density environment implies them to be interesting regions for studying the influence of cosmic environment on the formation of galaxies.

We will address the last two aspects in more detail below, along with a discussion of the available observational information on the dynamics of voids. A more focussed discussion of void evolution and dynamics within the context of the Cosmic Web is the subject of Sect. 4.

Void Dynamics

The essential role of voids in the organization of the cosmic matter distribution was recognized soon after their discovery [84]. This also includes their dynamical influence. As a result of their underdensity voids represent a region of weaker gravity, resulting in an effective repulsive peculiar gravitational

influence. Various studies have indeed found strong indicatations for their imprint in the peculiar velocity flows of galaxies in the Local Universe.

Bothun et al. [24] made the first claim of seeing pushing influence of voids when assessing the stronger velocity flows of galaxies along a filament in the first CfA slice. Stronger evidence came from the extensive and systematic POTENT analysis of Mark III peculiar galaxy velocities [194] in the Local Universe [19, 46]. POTENT found that for a fully selfconsistent reconstruction of the dynamics in the Local Universe, it was inescapable to include the dynamical influence of voids (see e.g. Dekel [47]). The DTFE maps by Romano-Díaz and van de Weygaert [149] of the density and velocity field in the Local Universe obtained from the PSCz redshift sample [25] do provide a very clear visual image of the influence of such voids in the Local Universe, with the pushing influence of the Sculptor void at the Local Supercluster as most outstanding example (see Fig. 10).

With the arrival of new and considerably improved data samples the dynamical influence of voids in the Local Universe has been investigated and understood in greater detail. The reconstruction of the density and velocity field in our local cosmos on the basis of the 2MASS redshift survey has indeed resulted in a very interesting and complete view of the dynamics on Megaparsec scales. As one may infer from Fig. 11 the repulsive influence of the Local Void is impressively strong and outstanding. This conclusion goes along with the conclusions reached on the basis of an extensive and careful analysis of the peculiar velocity of the Local Group by Tully et al. [184]. They are lead to the conclusion that the Local Void is responsible for a considerable repulsive influence, accounting for ~ 259 km s^{-1} of the ~ 631 km s^{-1} Local Group motion with respect to the CMB. While partly dependent on the details of the analysis, it seems hard to avoid the conclusion that we do not feel the presence of voids in our universe.

Voids and the Cosmos

Voids may function as probes of global cosmological parameters and on the underlying cosmology. Their intrinsic structure and shape, the outflow velocities and the corresponding redshift distortions are related to various aspects of the underlying cosmology. The outflow from the voids depends on the matter density parameter Ω_m, the Hubble parameter $H(t)$ and possibly on the cosmological constant Λ (see e.g. Van de Weygaert and van Kampen [187], Martal and Wassermann [111], Dekel and Rees [50], Bernardeau et al. [17], Fliche and Triay [61]). These parameters also dictate their redshift space distortions [154, 163].

Another interesting link between void structure and cosmology has recently been emphasized by Park and Lee [127] and Lee and Park [103]. They found that the intrinsic structure and shape of voids are sensitive to various aspects of the power spectrum of density fluctuations, including the imprint of dark energy.

The cosmological ramifications of the reality of a supersized void akin to the identified by Rudnick et al. [151] in the NVVS radio source counts would obviously be far-reaching.

Void Galaxies

A major point of interest concerns the galaxies within the voids, the void galaxies. Voids provide a unique and still largely pristine environment for studying the evolution of galaxies [80, 105, 131] and may represent a major challenge for current scenarios of structure formation. Peebles [131] pointed out that the observed salient and total absence of dwarf galaxies in nearby voids – for example the absence of dwarfs in the Local Void noticed by Karachentseva et al. [91] - could possibly involve strong ramifications for the viability of the ΛCDM cosmology on small scales.

A clear picture of the relation between void galaxies and their surroundings is just becoming available, be it there is still a lot of uncertainty concerning the physics which drives the observed correlations. The simplest models of biased galaxy formation (e.g Little and Weinberg [105]) predict that voids would be filled with galaxies of low luminosity, or galaxies of some other uncommon nature [80]. More sophisticated models have recently been developed [14, 64, 78, 116]; in these models the properties of galaxies are determined by the halos they inhabit. The recent interest in environmental influences on galaxy formation has prodded substantial activity in this direction [29, 74, 75, 81, 91, 101, 128, 140, 148, 178, 181].

2.4 Cosmic Shear and the Cosmic Web

The cosmic web is first and foremost defined and outlined by the dark matter distribution, the gravitationally dominant component which sets the corresponding gravitational potential. Galaxies are assumed to trace the underlying dark matter distribution. Even though the galaxies do indeed seem to provide a reasonable impression of the matter distribution, a direct map of the dark matter itself would obviously allow a real and unbiased view of the dynamics of the cosmic web.

A recent study has indeed managed to reveal the spatial dark matter distribution through its effect on the paths of the photons as they move through the Universe, meanwhile confirming that galaxies and starlight are in fact good tracers. Massey et al. [114] succeeded in producing the first truely three-dimensional map of the dark matter distribution. Their study is based on (weak) gravitational lensing data from the Cosmic Evolution Survey (COSMOS), and concerns a total region of 1637 square degrees meticulously observed by the ACS camera onboard the HST. An accurate and detailed two-dimensional map of the projected mass distribution clearly reveals the filamentary features connecting the high-density clusters (Fig. 13). Until recently,

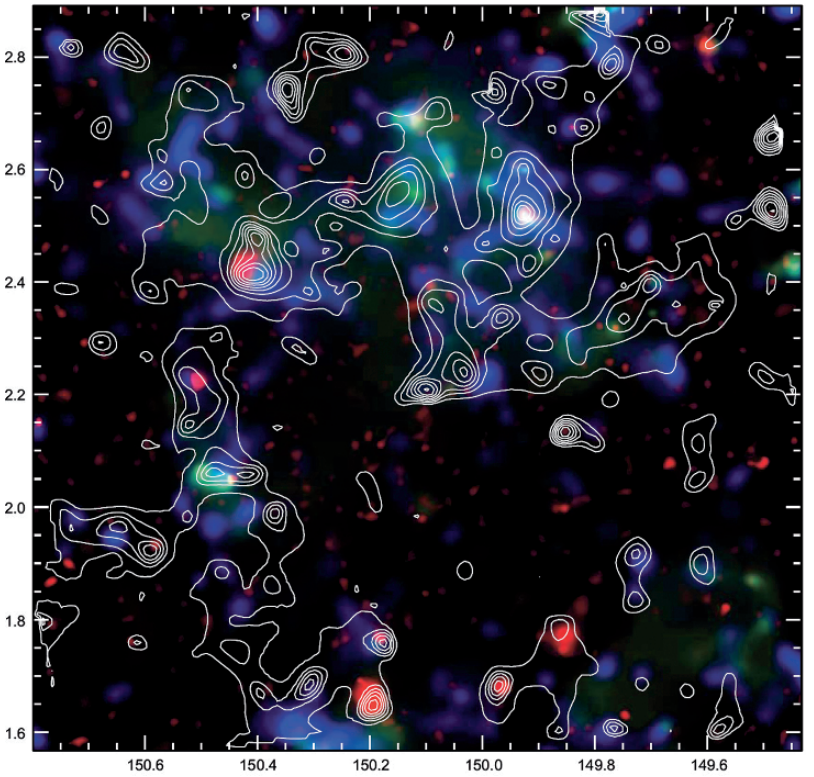

Fig. 13. The total projected matter density inferred from the large weak lensing study of the COSMOS data, shown in contours. The projected mass is dominated by dark matter. For comparison the matter surface density contours are superimposed on tracers of the baryonic matter distribution: (1) blue, the stellar mass (within $\Delta z \approx 0.1$) (2) yellow: the galaxy number density (within $\Delta z \approx 0.1$) and (3) red: hot dense gas, seen by deep X-ray observations with the XMM satellite. The X-ray emission by point sources has been removed. The dark matter reveals filamentary overdense regions that are topologically connected but insufficiently dense to generate X-ray emission: a loose network of filaments tracing the Cosmic Web. Within the filamentary network we recognize the dense compact cluster nodes. The most prominent peak in all four tracers is a single cluster of galaxies at $z = 0.73$ (α, δ=149 h,55 min, 2°31'). Courtesy of Richard Massey, also see Massey et al. [114]. Reproduced by permission of Nature

such weak lensing mass reconstructions were confined to the high-density regions in and around clusters because of the outstanding strength of their lensing signal. With the COSMOS map probing the more moderately dense regions of the cosmic web it turns out that stellar mass and galaxy number density do indeed accurately follow the dark matter distribution while the correlation with the X-ray emission – confined to the inner regions of clusters – is significantly less pronounced.

By complementing the lensing data with redshifts of the galaxy sources a tomographic analysis of the data, involving the assessment of the differential growth of the lensing signal between many thin slices separated by $\Delta z = 0.05$, made it possible to reconstruct the full three-dimensional matter distribution (Fig. 14). It did reveal that the massive cluster at $z = 0.73$ ($\alpha, \delta = 149$ h, 55 min, 2°31') is embedded within a giant three-dimensional structure which includes at least one filament.

The 3-D dark matter map is truely historical in that it uncovered for the first time the reality of a weblike pattern in the dark matter underlying the one that we see in the galaxy distribution. The potential for this new light

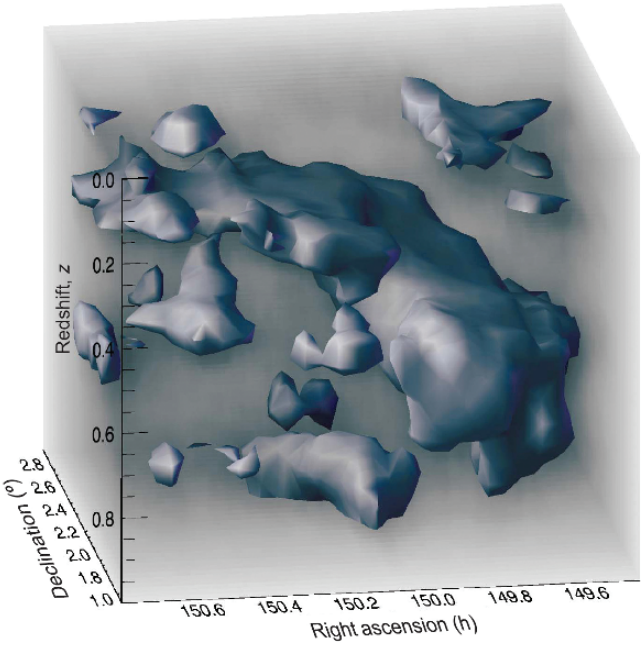

Fig. 14. Three-dimensional reconstruction of the dark matter distribution. The three axes correspond to right ascension, declination and redshift: with distance increasing towards the bottom. The redshift scale is highly compressed and the survey volume is really an elongated cone. The isodensity contour corresponds to a level of $1.4 \times 10^{13} M_{\odot}$ within a circle of radius 700 kpc and $\Delta z = 0.05$, arbitrarily chosen to highlight the filamentary structure. The 3-D map has been inferred from the tomographic analysis of the COSMOS weak lensing data, involving the assessment of the differential growth of the lensing signal between many thin slices separated by $\Delta z = 0.05$. The 3-D map reveals that the massive $z = 0.73$ cluster is indeed part of much larger 3-D structure, including a filament partially aligned along the line of sight. Courtesy of Richard Massey, also see Massey et al. [114]. Reproduced by permission of Nature

on the dark side of the Universe is tremendous. The detected filamentary DM network provides a direct and transparent link to theories of structure formation, directly tying in with collisionless dark matter and gravity without the necessity to involve complex and as yet not fully understood hydrodynamic, radiative and starformation processes.

2.5 The Gaseous Cosmic Web

Galaxies are assumed to trace the underlying dark matter distribution, and their spatial distribution (still) represents the most detailed and clearest outline of its intricate weblike features which we have available. Nonetheless, stars and galaxies do in fact represent only a minor fraction of all the baryons in the Universe. As far as baryons are concerned the cosmic web is first and foremost an intricate network of diffuse gaseous lanes pervading the Universe (see Fig. 16).

In other words, while in practice galaxies are used as tracers, it is the diffuse intergalactic medium (IGM) which forms the main baryonic constituent of the cosmic web. At high redshift ($z \gtrsim 2$) the overwhelming majority of baryons are in a diffuse, photoionized intergalactic medium, partly enriched by the products of stellar nucleosynthesis. This gas is observable as HI absorption lines in the spectra of distant background quasars (see Rauch [143], Cen et al. [30]). The resulting redshifted Lyman α (Lyα) absorption along their line of sight produces the Lyα forest, which represents a highly sensitive *one-dimensional* probe of the (gaseous) cosmic web (see Fig. 15). By the current epoch, hierarchical structure formation has produced deep potential wells into which the baryons accrete, thereby moving a significant portion of the baryons from the IGM into stars, galaxies, groups and clusters. Hydrodynamical simulations of cosmic structure formation have indicated that a significant fraction of the baryons at $z \sim 0$ are found in a gaseous form. The gas around emerging clusters falls into their potential wells and turns into hot highly ionized X-ray emitting intracluster gas. Most of the gas, with a temperature between 10^5 and 10^7 K, is found in regions of moderate overdensities $\delta \sim 10$–100. Part of this gas is associated with the virial regions around galaxies, accounting for around $\Omega_b \sim 0.024$ of the total $\Omega_b = 0.045$ contributed by baryons to the density of the Universe [63]. The remaining component of this diffuse Warm-Hot Intergalactic Medium (WHIM) mostly traces out the filamentary features in the cosmic web. It may account for a significant fraction of the missing baryons at low redshifts (Fukugita et al. [62] Fukugita & Peebles [63]). Probably there is also a significant amount of low temperature WHIM with $T < 10^5$ K, distributed mostly as sheet-like structures (Kang et al. [90]). The WHIM may even account for up to 30%–40% of the baryonic mass in the Universe (Davé et al. [42]). Its evolution is driven primarily by shock heating as the gas falls into the gravitationally generated potential wells, mainly those defined by the nonequilibrium large-scale structures such as filaments. For the heating of the

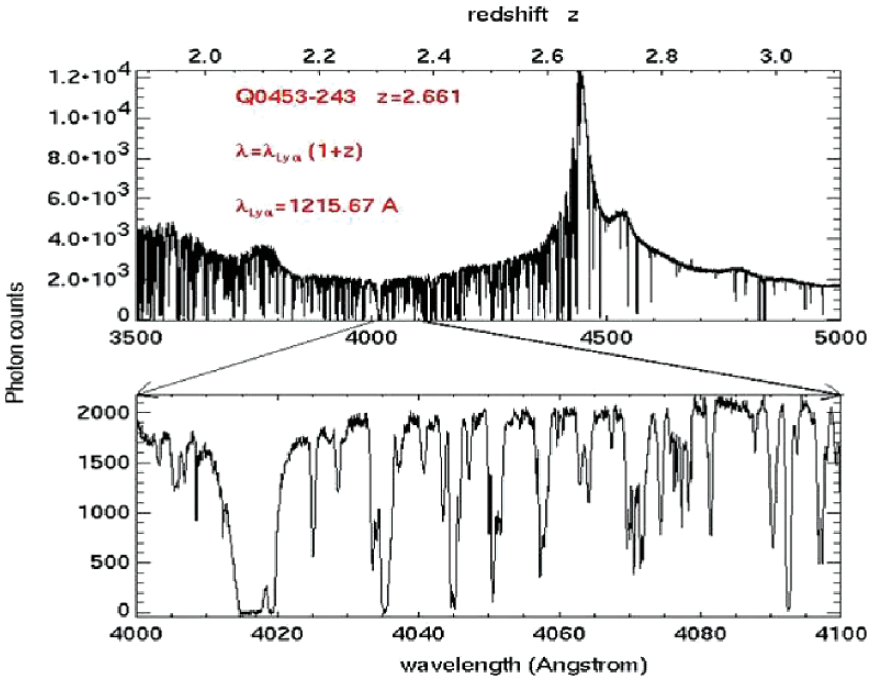

Fig. 15. The spectrum of the quasar Q0453-243 obtained with the HIRES spectrograph on the Keck I telescope. The quasar has an emission redshift of $z = 2.661$. To the left of the Lymanα emission line you see the "forest" of HI absorption lines produced by intervening, tenuous intergalactic clouds. The lower panel zooms in on the region between 4000 and 4100 A. The particularly strong line at 4020 A is a "damped Lymanα absorption feature produced in a cloud which is optically thick in HI. Image courtesy of Matteo Viel

gas, processes like supernova feedback, radiative cooling and photoionization are only of secondary importance.

The shock-heated WHIM gas in filaments and sheets is manifested best through emissions and absorptions in soft X-ray and far UV. It will make significant contributions to the soft X-ray background, and can be detected through absorptions of highly ionized species suchs as OVII and OVIII in AGN spectra and line emissions from OVII and OVIII ions. Detection of WHIM absorption in X-ray observations were reported by various groups (Kaastra et al. [86], Nicastro et al. [121]), while there was also a report of a possible detection of WHIM emission from a filament around Coma (Finoguenov [60]).

The study of the IGM represents an impressively rich source for our understanding of the cosmic web. Potentially the intricate structure can be traced in much more detail than by means of the discrete galaxy distribution. Different chemical species and ionization stages probe different density and temperature regimes within the cosmic web, which in turn may be related

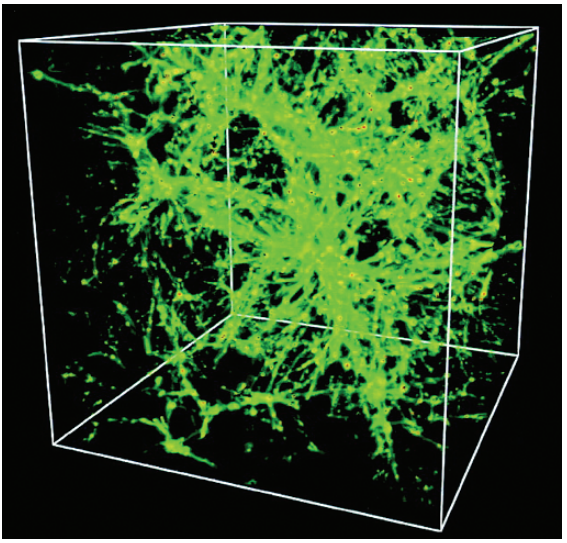

Fig. 16. Spatial distribution of the warm/hot intergalactic gas (WHIM) with temperature in the range $10^5 - 10^7$ K, at $Z = 0$, in a box of 85 h^{-1}Mpc. The image reveals the striking pattern of the Cosmic Web into which the WHIM gas has settled itself as it flowed into the potential wells set by the dark matter distribution. The green regions have densities about 10–20 times the mean baryon density of the universe at $Z = 0$; the yellow regions have densities about 100 times the mean baryon density, while the small isolated regions with red and saturated dark colours have even higher densities reaching about 1000 times the mean baryon density and are sites for current galaxy formation. Image courtesy of Renyue Cen, also see Cen and Ostriker [31]. Reproduced by permission of the AAS

to different regimes and stages of galaxy formation. However, in particular the most directly accessible study of the IGM, that of absorption line studies, is confined to one-dimensional probes. This renders it difficult to translate these to a three-dimensional image (yet, a constrained inversion is not entirely unfeasible, see Pichon et al. [132]). Emission line studies of the WHIM would offer the exciting potential of mapping the cosmic web through its gaseous contents. A meticulous detailed mapping comparable to that traced by the galaxy distribution remains as yet only a remote possibility.

3 Spatial Structure, Pattern Analysis and Object Identification

Many attempts to describe, let alone identify, the features and components of the Cosmic Web have been of a mainly heuristic nature. There are various relevant issues. The primary issue is that of defining a technique that sensitively probes the properties of the Cosmic Web. Another major point

of concern involves the sampling of the web patterns, by default limited in scope. Cosmological theories generally describe the development of structure in terms of continuous (dark matter) density and velocity fields. To a large extent our knowledge stems from a discrete sampling of these fields.

In the real world it is impossible to get exhaustive values of data at every desired point of space. The product of astronomical observations, physical experiments and computer simulations often concern data sets in two, three or more dimensions. This may involve the value of some physical quantity: the galaxy density field, the dark matter density field or the peculiar velocity field are amongst the best known examples. Often these are measured or determined from an irregularly distributed set of reference points.

The principal task for any formalism that seeks to process the sampled data on the cosmological matter distribution is to optimally retain or extract the required information on the Cosmic Web. Dependent on the purpose of a study, various different strategies may be followed:

- *Statistical Analysis*

  One strategy is to distill various statistical measures, or other sufficiently descriptive cosmological measures, which characterize specific aspects of the large scale matter distribution. In essence this involves the compression of the available information into a restricted set of parameters or functions, with the intention to compare or relate these to theoretical predictions.

- *Feature Identification*

  The identification and isolation of features and objects in the cosmic matter distribution – clusters, filaments and voids – is essential for understanding the nature of structures which form in the Universe and provides an important link between observation and theoretical models. On the one hand this may involve a cosmographic study of individual structures in our Cosmic neighbourhood. Their detail usually forms a welcome complement to surveys of large samples of similar objects, while sometimes they highlight the extremes in the cosmological zoo. Perhaps most important is the necessity of well-defined feature identifiers for proper statistical studies of cosmic structure formation.

- *Structure Reconstruction*

  For the determination of various statistical characterizations of cosmic structure it is imperative to define an optimal reconstruction of cosmic density and velocity fields. Demanding in itself, such a reconstruction is often complicated by the usually *discrete* nature of the sample point distribution and the highly inhomogeneous nature of the sample point distribution. The translation into a continuous field which optimally reflects reality is a far from trivial procedure and forms the subject of an extensive literature in computer science, visualization and applied sciences.

3.1 Statistics of the Cosmic Web

There is a variety of statistical measures characterizing specific aspects of the large scale matter distribution (for an extensive and complete review see Martínez & Saar, [112]). Below we list a selection of methods for structure characterisation and finding. It is perhaps interesting to note two things about this list:

(a) each of the methods tends to be specific to one particular structural entity
(b) there are no explicit wall-finders.

Both issues emphasize an important property that generic techniques for tracing structural features should possess (see 3.2). The skeleton formalism [122, 171, 172] accomplished this by tracing the mathematically well-defined skeleton of the Cosmic Web and arguing its close relationship to its filamentary constituents. More generic is the Scale Space approach adopted by Aragón-Calvo [5] (also see Aragón-Calvo et al. [6]): it provides a uniform approach to finding Blobs, Filaments and Walls as individual objects that can be catalogued and studied.

Structure from Higher Moments

The clustering of galaxies and matter is most commonly described in terms of a hierarchy of correlation functions. The two-point correlation function (and its Fourier transform, the power spectrum) remains the mainstay of cosmological clustering analysis and has a solid physical basis. However, the nontrivial and nonlinear patterns of the cosmic web are mostly a result of the phase correlations in the cosmic matter distribution [32, 38, 153]. While this information is contained in the moments of cell counts [44, 65, 130] and, more formally so, in the full hierarchy of M-point correlation functions ξ_M, their measurement has proven to be impractical for all but the lowest orders [85, 130, 177].

The Void probability Function [102, 193] provided a characterisation the "voidness" of the Universe in terms of a function that combined information from many higher moments of the point distribution. But, again, this has not provided any identification of individual voids.

Topological Methods

The shape of the local matter distribution may be traced on the basis of an analysis of the statistical properties of its inertial moments [8, 12, 110]. These concepts are closely related to the full characterization of the topology of the matter distribution in terms of four Minkowski functionals [117, 162]. They are solidly based on the theory of spatial statistics and also have the great advantage of being known analytically in the case of Gaussian random fields. In particular, the *genus* of the density field has received substantial

attention as a strongly discriminating factor between intrinsically different spatial patterns [69, 82].

The Minkowski functionals provide global characterisations of structure. An attempt to extend its scope towards providing locally defined topological measures of the density field has been developed in the SURFGEN project defined by Sahni and Shandarin and their coworkers [158, 164]. The main problem remains the user-defined, and thus potentially biased, nature of the continuous density field inferred from the sample of discrete objects. The usual filtering techniques suppress substructure on a scale smaller than the filter radius, introduce artificial topological features in sparsely sampled regions and diminish the flattened or elongated morphology of the spatial patterns. Quite possibly the introduction of more advanced geometry based methods to trace the density field may prove a major advance towards solving this problem.

Importantly, Martínez et al. [113] and Saar et al. [155] have generalized the use of Minkowski Functionals by calculating their values in a hierarchy of scales generated from wavelet-smoothed volume limited subsamples of the 2dF catalogue. This approach is particularly effective in dealing with non-Gaussian point distributions since the smoothing is not predicated on the use of Gaussian smoothing kernels.

3.2 Structure Finding

In addition to the statistical characterization of the cosmic matter density field, a major effort goes into identifying and isolating features and individual structures in the cosmic matter distribution. The vast majority of these studies have focussed on the detection of clusters of galaxies. Tracing filamentary has gained relatively little attention, and with the exception of a few rare outstanding concentrations – the Great Wall [66] and the SDSS Great Wall [70] – the detection of sheets is a virtually nonexistent activity.

Cluster Finding

In the context of analyzing distributions of galaxies we can think of cluster finding algorithms. There we might define a cluster as an aggregate of neighbouring galaxies sharing some localised part of velocity space. Algorithms like HOP attempt to do this. However, there are always issues arising such as how to deal with substructure: that perhaps comes down to the definition of what a cluster is. Here we focus on defining coherent structures based on particle positions alone. The velocity space data is not used since there is no prior prejudice as to what the velocity space should look like.

Filament Finding

The connectedness of elongated supercluster structures in the cosmic matter distribution was first probed by means of percolation analysis, introduced

and emphasized by Zel'dovich and coworkers [197], while a related graph-theoretical construct, the minimum spanning tree of the galaxy distribution, was extensively probed and analysed by Bhavsar and collaborators [11, 34, 72] in an attempt to develop an objective measure of filamentarity.

Finding filaments joining neighbouring clusters has been tackled, using quite different techniques, by Colberg, Krughoff and Connolly [35] and by Pimbblet [133]. More general filament finders have been put forward by a number of authors. Stoica et al. [173] use a generalization of the classical Candy model to locate and catalogue filaments in galaxy surveys. This approach has the advantage that it works directly with the original point process and does not require the creation of a continuous density field. However, it is very computationally intensive.

The mathematically most rigorous program for filament description and analysis is that of the skeleton analysis of density fields by Novikov, Colombi and Doré [122] (2-D) and Sousbie et al. [17] (3-D). Based on Morse theory (see Colombi, Pogosyan and Souradeep [40]) the skeleton formalism analyzes continuous density fields and detects morphological features – maxima and saddle points in the density field – by relating density field gradients to the Hessian of the density field (also see Doré et al. [52]). It results in an elegant and effective tool with a particular focus towards tracing the filamentary structures in the cosmic web. However, it is computationally intensive and may be sensitive to the specific method of reconstruction of the continuous density field. The Hessian of the density field also forms the basis of the MMF analysis developed by Aragon-Calvo [5] (see Fig. 17) although MMF embeds this within a formalism that explicitly adresses the multiscale character of the cosmic density field and includes the shape conserving abilities of the tessellation based density field reconstruction Schaap and van de Weygaert [161].

Void Finding

Voids are distinctive and striking features of the cosmic web, yet identifying and tracing their outline within the complex spatial geometry of the Cosmic Web has proven to be far from trivial. There have been extensive searches for voids in galaxy catalogues [81, 139] and in numerical simulations [4, 7].

Several factors contribute to making systematic void-finding difficult. One major obstacle is that there is not an unequivocal definition of what a void is and as a result there is considerable disagreement on the precise outline of such a region (see e.g. Shandarin et al. [165]). The fact that voids are almost empty of galaxies means that the sampling density plays a key role in determining what is or is not a void [163]. Moreover, void finders are often predicated on building void structures out of cubic cells [93] or out of spheres (e.g: Patiri et al. [129]). Because of the vague and diverse definitions, and the diverse interests in voids, there is a plethora of void identification procedures [4, 7, 36, 56, 76, 81, 93, 129, 139, 165]. For example, there are methods that attempt to synthesize voids from the intersection of cubic or spherical elements and

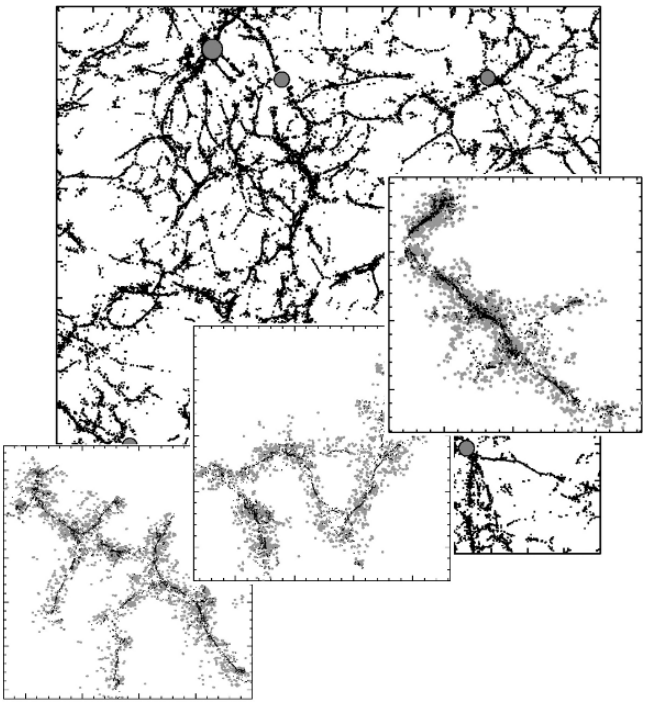

Fig. 17. The filamentary network in a GIF ΛCDM simulation. The filaments were identified by means of the MMF technique of Aragón-Calvo et al. [6]. The filled (grey) circles correspond to clusters with a mass above 10^{14} $M_{\odot}$. The inserts contain three specific examples of filaments. The gray dots represent the original (simulation) dark matter particles. The spine of the filaments (black particles) is the result of the filament compression algorithm of Aragón-Calvo [5]. Image courtesy M. Aragón-Calvo, also see Aragón-Calvo [5]

do so with varying degrees of success. The *Aspen-Amsterdam Void Finder Comparison Project* of Colberg et al. [37] will clarify many of these issues. The Watershed-based algorithm of Platen, van de Weygaert and Jones [135] aims to avoid issues of both sampling density and shape.

3.3 Reconstruction of the Cosmic Web

For a meaningful analysis and interpretation of spatial data it is often necessary to obtain estimates of the related field values throughout the sample volume. The *reconstructed* continuous field may subsequently be processed in order to yield a variety of interesting parameters. Ideally, reconstruction procedures should be based upon solid statistical foundations. The complex reality of the cosmic web – marked by asymmetric and anisotropic features and a large range of densities– renders it very difficult to develop and infer

statistical methods from first principle. The work by Erdoğdu et al. [58] and Kitaura and Enßlin [98] represent examples of possibly rewarding strategies.

In the observational reality galaxies are the main tracers of the cosmic web and it is mainly through the measurement of the redshift distribution of galaxies that we have been able to map its structure. Another example is that of the related study of cosmic flows in the nearby Universe, based upon the measured peculiar velocities of a sample of galaxies located within this cosmic volume. Likewise, simulations of the evolving cosmic matter distribution are almost exclusively based upon N-body particle computer calculation, involving a discrete representation of the features we seek to study. Both the galaxy distribution as well as the particles in an N-body simulation are examples of *spatial point processes* in that they are

- *discretely sampled*
- have an *irregular spatial distribution.*

A major part of any reconstruction procedure is the filtering and interpolation of the measured data.

3.4 Spatial Data: Filtering and Interpolation

Issues of *smoothing* and *spatial interpolation* of the measured data over the sample volume are of considerable importance and interest in many different branches of science. Interpolation is fundamental to graphing, analysing and understanding of spatial data. Key references on the involved problems and solutions include those by Ripley [147], Sibson [170], Watson [192], Cressie [41]. While of considerable importance for astronomical purposes, many available methods escaped attention. A systematic treatment and discussion within the astronomical context is the study by Rybicki and Press [152], who focussed on linear systems as they developed various statistical procedures related to linear prediction and optimal filtering, commonly known as Wiener filtering. An extensive, systematic and more general survey of available mathematical methods can be found in a set of publications by Lombardi and Schneider [106–108].

DTFE: Delaunay Tessellation Field Estimator

A particular class of spatial point distributions is the one in which the point process forms a representative reflection of an underlying smooth and continuous density/intensity field. The spatial distribution of the points itself may then be used to infer the density field. This forms the basis for the interpretation and analysis of the large scale distribution of galaxies in galaxy redshift surveys. The number density of galaxies in redshift survey maps and N-body particles in computer simulations is supposed to be proportional to the underlying matter density.

One noteworthy example of a technique which uses this fact is the *DTFE* method, a linear version of *natural neighbour* interpolation. The DTFE technique [161, 188] recovers fully volume-covering and volume-weighted continuous fields from a discrete set of sampled field values. The method has been developed by Schaap and van de Weygaert [161] and forms an elaboration of the velocity interpolation scheme introduced by Berhardeau and van de Weygaert [16]. It is based upon the use of the Voronoi and Delaunay tessellations of a given spatial point distribution to form the basis of a natural, fully self-adaptive filter in which the Delaunay tessellations are used as multidimensional interpolation intervals. An example is the void density and velocity field in Fig. 24.

The primary ingredient of the DTFE method is the Delaunay tessellation of the particle distribution. The Delaunay tessellation of a point set is the uniquely defined and volume-covering tessellation of mutually disjunct Delaunay tetrahedra (triangles in 2D). Each is defined by the set of four points whose circumscribing sphere does not contain any of the other points in the generating set [51]. The Delaunay tessellation and the Voronoi tessellation of the point set are each others *dual*. The Voronoi tessellation is the division of space into mutually disjunct polyhedra, each polyhedron consisting of the part of space closer to the defining point than any of the other points [123, 191].

DTFE exploits three properties of Voronoi and Delaunay tessellations [160, 188]. The tessellations are very sensitive to the local point density. DTFE uses this to define a local estimate of the density on the basis of the inverse of the volume of the tessellation cells. Equally important is their sensitivity to the local geometry of the point distribution. This allows them to trace anisotropic features such as encountered in the cosmic web. Finally, DTFE exploits the adaptive and minimum triangulation properties of Delaunay tessellations in using them as adaptive spatial interpolation intervals for irregular point distributions. In this way it is the first order version of the *Natural Neighbour method* [27, 169, 174, 184].

Within the cosmological context a major – and crucial – characteristic of a processed DTFE density field is that it is capable of delineating three fundamental characteristics of the spatial structure of the megaparsec cosmic matter distribution. It outlines the full hierarchy of substructures present in the sampling point distribution, relating to the standard view of structure in the Universe having arisen through the gradual hierarchical buildup of matter concentrations. DTFE also reproduces any anisotropic patterns in the density distribution without diluting their intrinsic geometrical properties. This is particularly important when analyzing the the prominent filamentary and planar features marking the Cosmic Web. A third important aspect of DTFE is that it outlines the presence and shape of voidlike regions. Because of the interpolation definition of the DTFE field reconstruction voids are rendered as regions of slowly varying and moderately low density values.

Multiscale Morphology Filter

Recently a variety of methods have been developed towards a complete morphological analysis of the cosmic web in the cosmic matter distribution. Perhaps the most rigorous program, with a particular emphasis on the description and analysis of filaments, is that of the *skeleton* analysis of density fields by Novikov, Colombi and Doré [122] (2-D) and Sousbie et al. [172] (3-D) (see Sect. 3.2). Another strategy has been followed by Hahn et al. [76]. They identify clusters, filaments, walls and voids in the matter distribution on the basis of the tidal field tensor $\partial^2\phi/\partial x_i \partial x_j$, determined from the density distribution filtered on a scale of $\approx 5\,\mathrm{h}^{-1}$ Mpc. Here we shortly focus on the Multiscale Moprhology Filter (MMF), introduced by Aragón-Calvo et al. [5]. The MMF dissects the cosmic web on the basis of the multiscale analysis of the Hessian of the density field.

Figure 18 contains a schematic overview of the Multiscale Morphology Filter (MMF) to isolate and extract elongated filaments (dark grey), sheetlike walls (light grey) and clusters (black dots) in the weblike pattern of a cosmological N-body simulation Aragón-Calvo et al. [6]. The first stage is the translation of a discrete particle distribution (top lefthand frame) into a DTFE density field (top centre). This guarantees a morphologically unbiased and optimized density field retaining all features visible in a discrete galaxy

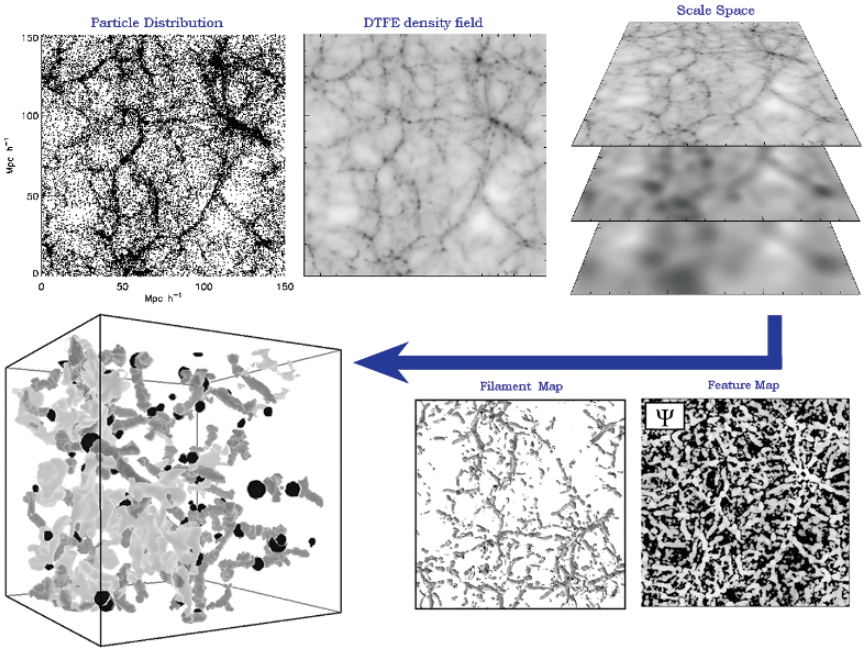

Fig. 18. Scheme of the Multiscale Morphology Filter for extracting weblike morphologies. See text for explanation. From van de Weygaert and Schaap [188]

or particle distribution. The DTFE field is filtered over a range of scales (top righthand stack of filtered fields). By means of morphology filter operations defined on the basis of the Hessian of the filtered density fields the MMF successively selects the regions which have a bloblike (cluster) morphology, a filamentary morphology and a planar morphology, at the scale at which the morphological signal is optimal. This produces a feature map (bottom left-hand). By means of a percolation criterion the physically significant filaments are selected (bottom centre). Following a sequence of blob, filament and wall filtering finally produces a map of the different morphological features in the particle distribution (bottom lefthand). The 3-D isodensity contours in the bottom lefthand frame depict the most pronounced features (also see Fig. 17).

MMF and the Cosmic Web

Two noteworthy recent results obtained by MMF concerns the inventory of mass and volume content of the Cosmic Web [5], shown in Fig. 19. The results relate to the present-day epoch in a ΛCDM N-body simulation. Clusters occupy the smallest volume fraction in the cosmic web, accounting for only 0.4%. They do, however, represent a major share of the mass (28%), making them by far the densest components of the Cosmic Web. Most mass (39%) in the Universe resides in filaments, tracing out almost 10% of the total volume. Sheet contain only a small fraction of the mass, $\approx 5.5\%$ and occupy a relatively small volume (4.9%), making them the most tenuous structures in the Cosmic Web.

Also highly relevant is the issue of the connection between filaments and clusters. The number of filaments emanating from a cluster turns out to be a strong function of the cluster mass (see Fig. 20). More massive clusters are connected to considerably more filaments: MMF analysis indicates that

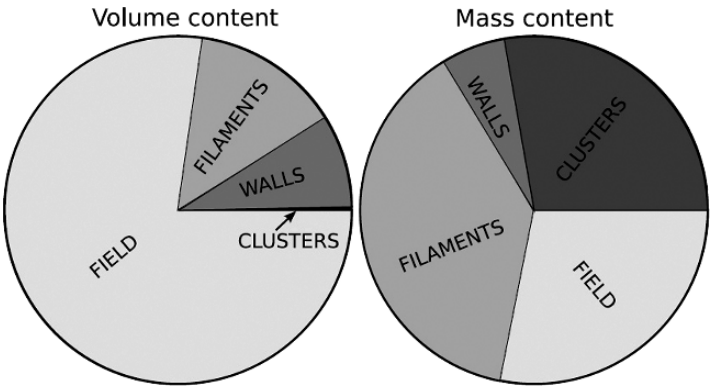

Fig. 19. Pie diagram showing an inventory of the Cosmic Web in terms of volume (**left**) and mass (**right**). Image courtesy M. Aragón-Calvo, also see Aragón-Calvo [5]

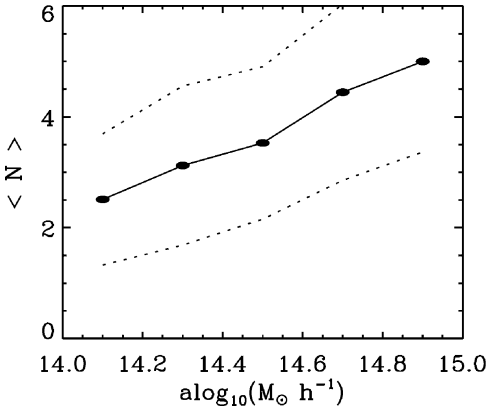

Fig. 20. Mean number of filaments as a function of the mass of the clusters to which they are connected (*solid line*). *Dotted line*: 1σ dispersion. Image courtesy M. Aragón-Calvo, also see Aragón-Calvo [5]

clusters with a mass $M \sim 10^{14}$ $M_\odot$ have on average 2 filaments connected to them, clusters with a mass $M \sim 10^{15}$ $M_\odot$ more than five filaments. Other studies have found a similar relation based on intracluster filaments found in N-body simulations [35] and visually identified filament-cluster connections from the 2dF galaxy redshift survey [133].

4 Voids

A manifest and prominent morphological aspect of the Megaparsec matter and galaxy distribution is the marked and dominant presence of large underdense regions, the *Voids*. A proper and full understanding of the formation and dynamics of the Cosmic Web is not possible without understanding the structure and evolution of voids. With respect to their role in the structure and buildup of the Cosmic Web we need to address three crucial aspects of void evolution:

- *Formation and Evolution of Voids*
  Voids form in and around density troughs in the primordial density field. As a result of the corresponding weaker internal gravity matter matter streams out of the interior of voids while the void as a whole will expand with respect to the background Universe.
- *Void Dynamics and Void Outflow*
  As a result of their underdensity voids represent a region of weaker gravity. This results in an effective repulsive gravitational influence. Various galaxy redshift surveys and studies of galaxy peculiar velocities have indeed uncovered this imprint in the cosmic velocity flow in the Local Universe (see Sect. 2.3).

- *Void Hierarchy and Substructure*
  Not only galaxies, galaxy halos and clusters of galaxies get assembled in a hierarchical fashion. Also the buildup of voids proceeds via a complex and intricate process of hierarchical evolution. Insight into this evolution is essential for understanding the overall geometry and structure of the Cosmic Web. The remnants of the hierarchical void evolution can still be seen when studying the observed spatial galaxy distribution or when analyzing N-body simulations of structure formation. It should also form the basis for the study of properties of the void galaxy population and the dependence on environment.

In the subsequent sections we will address each of these issues in some detail.

4.1 Formation and Evolution of Voids

Voids emerge out of the density troughs in the primordial Gaussian field of density fluctuations. Early theoretical models of void formation concentrated on the evolution of isolated voids [18, 20, 79, 84]. Initially underdense regions expand faster than the Hubble flow, and thus expand with respect to the background Universe. If they are not embedded within overdense regions, such regions eventually form voids which are surrounded by dense void walls. At any cosmic epoch the voids that dominate the spatial matter distribution are a manifestation of the cosmic structure formation process reaching a non-linear stage of evolution.

In a void-based description of the evolution of the cosmic matter distribution, voids mark the transition scale at which density perturbations have decoupled from the Hubble flow and contracted into recognizable structural features. On the basis of theoretical models of void formation one might infer that voids may act as the key organizing element for arranging matter concentrations into an all-pervasive cosmic network [84, 145, 168, 186]. As voids expand, matter is squeezed in between them, and sheets and filaments form the void boundaries. This view is supported by numerical studies and computer simulations of the gravitational evolution of voids in more complex and realistic configurations [36, 53, 68, 111, 125, 145, 187]. A marked example of the evolution of a typical large and deep void in a ΛCDM scenarios is given by the time sequence of six frames in Fig. 21.

Void Characteristics: an Inventory

The formation and evolution of voids involves a range of interesting and intricate processes and aspects. A listing of a dozen characteristic properties may elucidate this.

- *Voids expand.*
  The underdensity of a void corresponds to a weaker interior gravitational field. With respect to the global universe this leads to an effective (peculiar) gravity inducing a general flow out of the void region.

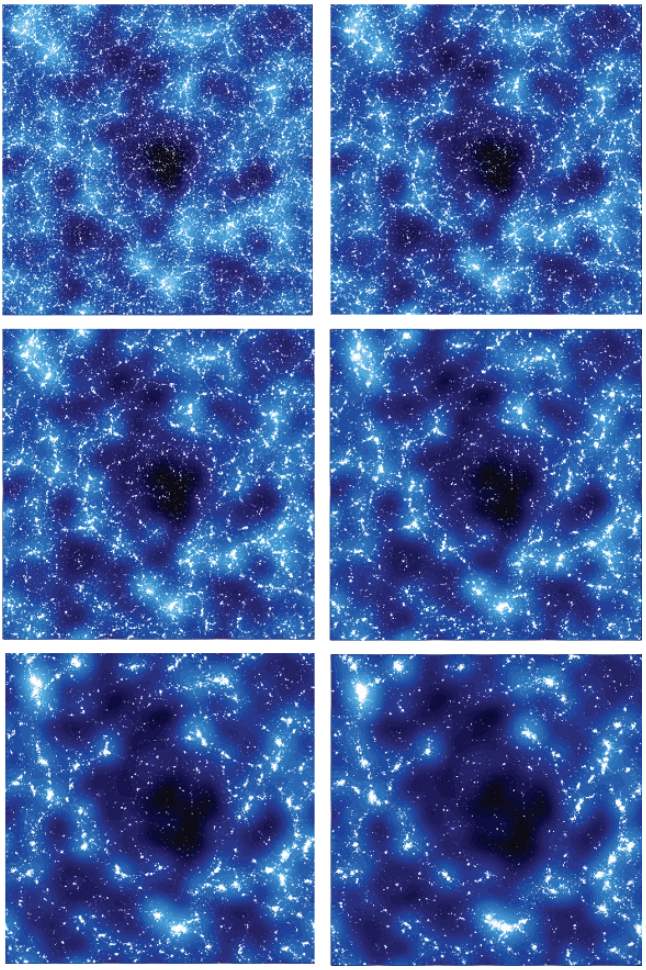

Fig. 21. Simulation of evolving void (LCDM scenario). Image courtesy of Erwin Platen

- *Voids empty.*
  As matter streams out of the void, the density within the void decreases. Isolated voids will asymptotically evolve towards an underdensity $\delta = -1$, pure emptiness.

- *Voids form ridges.*
  As the density within voids gradually increases outward, the corresponding peculiar (outward) gravitational acceleration decreases outward: void matter in the centre moves outward faster than void matter towards the boundary. As a result matter accumulates in ridges surrounding the void

(see Fig. 22). The steepness of the resulting density profile depends on the protovoid depression [126].

- *"Bucket" density profile*
  Voids assume a "bucket" shape – marked by a uniform interior density depression and a steep outer boundary – as a result of the fast outflow from the "flat" centre in a primordial underdensity. While their matter content accumulates near and around steep density ridges, the interior involves into a region resembling a low-density homogeneous FRW Universe (see Fig. 22).

- *Superhubble void expansion*
  Related to the uniform density interior of mature voids the corresponding peculiar velocity field is that of a "Superhubble" flow [84]: the interior flowfield of voids is marked by a uniform velocity divergence [160]. For a spherically symmetric void model it is rather straightforward to analytically infer that this is the expected natural tendency for voids (see Fig. 22). It is a manifestation of Birkhoff's theorem, according to which a void region can be described as an isolated lower Ω FRW universe [68, 187]. An analysis of N-body simulations by means of the DTFE technique has shown this also to be the case for the more complex situation of hierarchical structure formation (see Sect. 4.3).

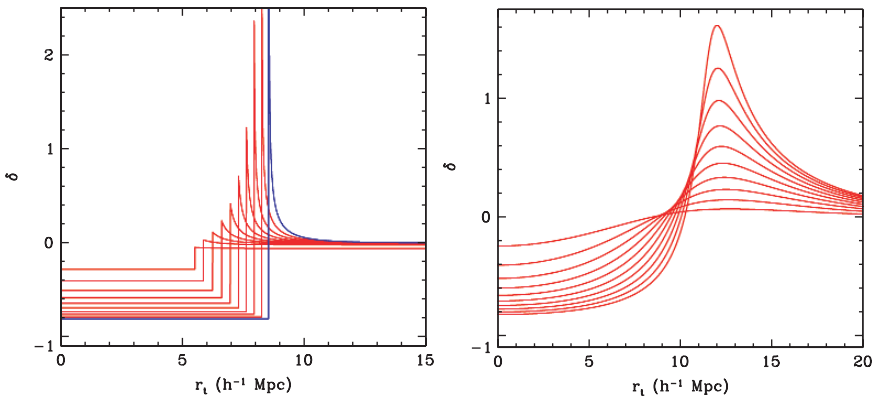

Fig. 22. Spherical model for the evolution of voids. **Left**: a pure (uncompensated) tophat void evolving up to the epoch of shell-crossing. Initial (linearly extrapolated) density deficit was $\Delta_{\rm lin,0} = -10.0$, initial (comoving) radius $\widetilde{R}_{i,0} = 5.0\ {\rm h}^{-1}$ Mpc. **Right**: a void with an angular averaged SCDM profile. Initial density deficit and characteristic radius are same as for the tophat void (**left**). The tendency of this void to evolve into a tophat configuration by the time of shell crossing is clear. Shell-crossing, and the formation of a ridge, happens only if the initial profile is sufficiently steep

- *Characteristic void and shellcrossing*
  Overdense spherical peaks have a characteristic and time of collapse, coincident with a linearly extrapolated density $\delta_c = 1.69$. Voids have a similar globally valid characteristic epoch of evolution, that of *shellcrossing*. This happens when interior shells of matter take over initially exterior shells. It happens when a primordial density depression attains a linearly extrapolated underdensity $\delta_v = -2.81$ (for EdS universe). A perfectly spherical "bucket" void will have expanded by a factor of 1.72 at shellcrossing, and therefore have evolved into an underdensity of $\sim 20\%$ of the global cosmological density, ie. $\delta = -0.8$.

- *Identity observed voids*
  Bertschinger's thesis work demonstrated that once voids have passed the stage of shellcrossing they enter a phase of self-similar expansion [18]. Subsequently, their expansion will slow down with respect to the earlier linear expansion. This impelled Blumenthal et al. [20] to identify voids in the present-day galaxy distribution with voids that have just reached the stage of shell-crossing.

- *Void shapes: spherical tendencies*
  Icke [84] pointed out that any (isolated) aspherical underdensity will become more spherical as it expands. The effective gravitational acceleration is stronger along the short axis than along the longer axes. For overdensities this results in a stronger inward acceleration and infall, producing increasingly flattened and elongated features. By contrast, for voids this translates into a larger *outward* acceleration along the shortest axis so that asphericities will tend to diminish. For the interior of voids this tendency has been confirmed by N-body simulations [187]. In reality, voids will never reach sphericity as a result of large scale dynamical and environmental factors [136].

- *Nonlinearity of voids*
  While by definition voids correspond to density perturbations of at most unity, $|\delta_v| \leq 1$, mature voids in the nonlinear matter distribution do represent *highly nonlinear* features. This may be best understood within the context of Lagrangian perturbation theory [157]. Overdense fluctuations may be described as a converging series of higher order perturbations, the equivalent perturbation series is less well behaved for voids. The successive higher order terms of both density deficit and corresponding velocity divergence alternate between negative and positive (see Fig. 23).

- *Dilution of void substructure*
  In hierarchical scenarios of structure formation void regions contain substantial amounts of infrastructure (see Sect. 4.4). The low-density environment of voids slows the growth of structure (for a thorough analytical

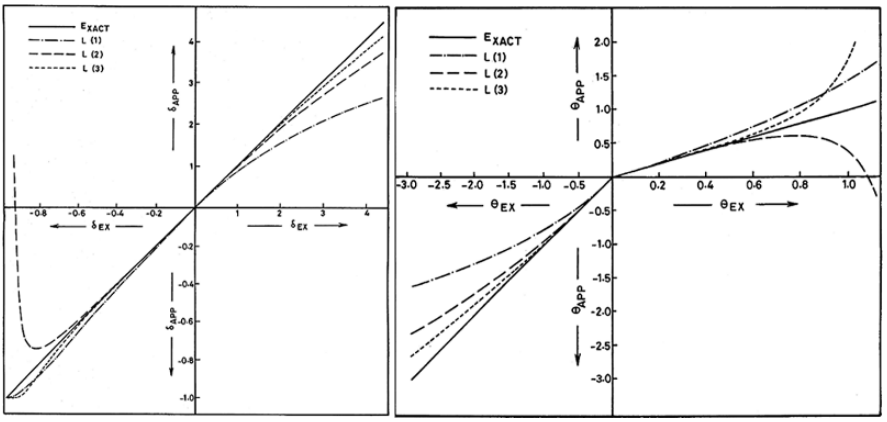

Fig. 23. Void nonlinearity in Lagrangian perturbation theory, from Sahni and Shandarin [157]. **Lefthand Frame**: density contrast $\delta_{\rm APP}$ in Lagrangian perturbation series $L(n)$ plotted against the exact tophat solution $\delta_{\rm EX}$ for underdense regions (**lower left**) and overdense regions (**upper right**). Whereas the accuracy of $L(n)$ increases with n when describing the behaviour of overdense regions, $L(n)$ wiht $N > 1$ do not fare as well when applied to underdense regions. Although for voids $L(n)$ with $n = 2, 3$ are initially more accurate than $L(1)$ (Zel'dovich approximation), their accuracy becomes poorer with time. Moreover, $L(2)$ shows pathological behaviour at late times when $\delta_{\rm EX} < -0.7$. Righthand frame: The dimensionless velocity divergence field $\theta_{\rm APP}$ in Lagrangian perturbation series $L(n)$ is shown plotted against the exact solution $\theta_{\rm EX}$, for overdense regions (**lower left**) and underdense regions (**upper right**). $l(n)$ with $n = 2, 3$ give better results than $l(a)$ for overdense but not for underdense regions. From Sahni and Shandarin [157]. Image courtesy of Sergei Shandarin

treatment see Goldberg and Vogeley [68]). The net result is a diluted and diminished infrastructure which remains visible, at ever decreasing density contrast, as cinders of the earlier phases of the *void hierarchy* in which the substructure stood out more prominent (see Sect. 4.8).

- *Collapse of voids*
  Instead of expanding, voids embedded in a larger scale environment of sufficient overdensity, or surrounded by structures effecting a strong enough tidal force field, may tend to collapse. This process of void collapse is especially relevant for small (sub)voids near the boundaries of large dominating voids. The process is of crucial importance in the hierarchical evolution of voids (see Sect. 4.8).

4.2 Void Identity and Maturity

One question of relevance is that of the identity of the observed voids. In other words, what defines a mature void? A reasonable answer may be found

on the basis of the spherical model. This teaches us that voids may be assigned a characteristic dynamical time, corresponding to a threshold of the linearly extrapolated primordial density field. A reasonable suggestion is that of a void reaching maturity at the moment of *shell-crossing*, ie. the stage at which the

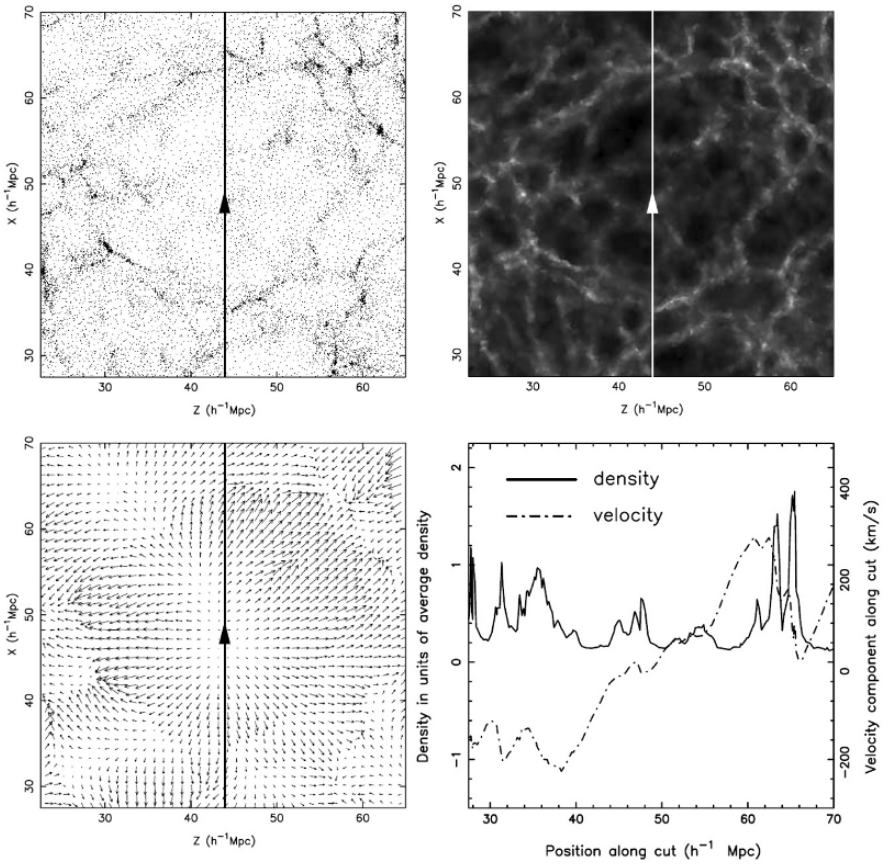

Fig. 24. The density and velocity field around a void in the GIF LCDM simulation. The top righthand panel shows the N-body simulation particle distribution within a slice through the simulation box, centered on the void. The top righthand panel shows the grayscale map of the DTFE density field reconstruction in and around the void, the corresponding velocity vector plot is shown in the bottom lefthand panel. Notice the detailed view of the velocity field: within the almost spherical global outflow of the void features can be recognized that can be identified with the diluted substructure within the void. Along the solid line in these panels we determined the linear DTFE density and velocity profile (**bottom righthand frame**). We can recognize the global "bucket" shaped density profile of the void, be it marked by substantial density enhancements. The velocity field reflects the density profile in detail, dominated by a global super-Hubble outflow. From Schaap [160]

inner shells of a void do overtake the outer shells as a result of their larger peculiar acceleration. Bertschinger [18] pointed out that a void would assume a self-similar expansion and propagate at a slower rate through the surrounding medium Bertschinger [18]. On the basis of this observation, Blumenthal et al. [20] suggested that the voids observed in galaxy redshift surveys, or in N-body simulations, should be identified with such shell-crossing voids.

The void threshold that corresponds to shell-crossing of a spherical tophat void, $\delta_v = -2.81$ (for a $\Omega_m = 1$ Einstein-de Sitter Universe, and for a growing-mode perturbation). Once the (fictitious) linear growth of a density trough in the primordial density field has reached the *void barrier* the depression will have evolved into a genuine void. Given the primordial density field $\delta(\mathbf{x})$, linearly interpolated to the present epoch, at any one cosmic redshift z one can identify the voids that have evolved beyond the shell-crossing phase and emerged as mature voids,

$$\Delta(\mathbf{x}) \,<\, \delta_{\rm ssc}(z, \Omega_m, \Omega_\Lambda) \,\approx\, \frac{\delta_{\rm v}}{D(z)}\,, \tag{1}$$

where the index *ssc* refers to "spherical shell crossing".

4.3 A Void in LCDM

Soon after their discovery, various studies pointed out their essential role in the organization of the cosmic matter distribution (e.g. icke [84], Regős and Geller [145]). Their effective repulsive influence over their surroundings has been recognized in various galaxy surveys in the Local Universe (see Sect. 2.3).

Here we address the void's dynamical influence by means of a case study of the structure and outflow from a void selected from a ΛCDM GIF N-body simulation Kauffmann et al. [94]. Figure 25 shows a typical void-like region in a ΛCDM Universe. It concerns a 256^3 particles GIF N-body simulation, encompassing a ΛCDM ($\Omega_m = 0.3, \Omega_\Lambda = 0.7, H_0 = 70\,$km/s/Mpc) density field within a (periodic) cubic box with length 141 h^{-1} Mpc and produced by means of an adaptive $\mathrm{P^3M}$ N-body code.

The top left frame shows the particle distribution in and around the void within this 42.5 h^{-1} Mpc wide and 1 h^{-1} Mpc thick slice through the simulation box. In the same figure we include panels of the density and velocity field in the void, determined by means of a DTFE reconstruction (see Schaap [160] van de Weygaert and Schaap [188]). Both form a nice illustration of the capacity of the tessellation-based DTFE interpolation and reconstruction technique to translate the inhomogeneous particle distribution into highly resolved continuous and volume-filling fields and even follow the density field as well as velocity flow throughout diluted void regions.

Void Infrastructure

The void region appears as a slowly varying region of low density (top right-hand frame). Notice the clear distinction between the empty(dark) interior

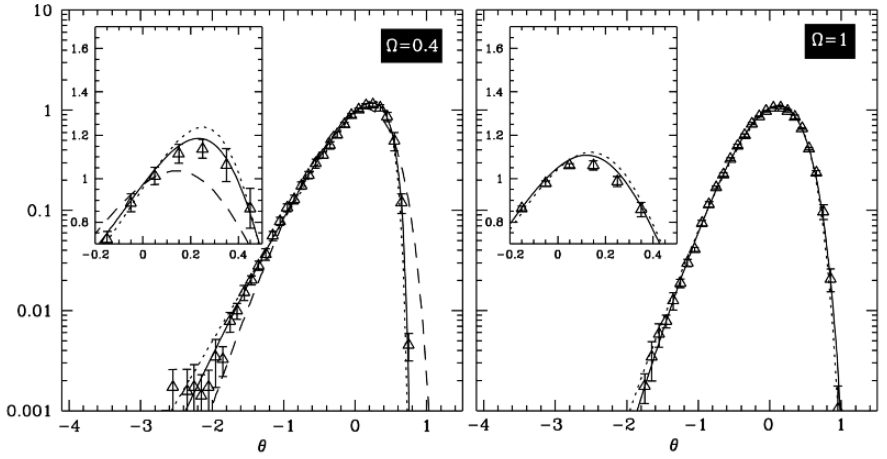

Fig. 25. The imprint of voids on the cosmic velocity field. The velocity divergence pdf for a matter-dominated $\Omega = 0.4$ and a $\Omega = 1.0$ universe, determined from a CDM N-body simulation by means of the DTFE technique. The pdf has a sharp high-value edge, defined by the outflow from voids. **Lefthand frame**: $\Omega = 0.4$, with superimposed (*dashed*) the pdf for a $\Omega = 1.0$ Universe. **Righthand frame**: $\Omega = 1.0$. From Bernardeau et al. [17]

regions of the void and its edges. In the interior of the void several smaller *subvoids* can be distinguished, with boundaries consisting of low density filamentary or planar structures.

The general characteristics of the expanding void are most evident when following the density and velocity profile along a one-dimensional section through the void. The bottom-left frame of Fig. 24 shows these profiles for the linear section along the solid line indicated in the other three frames. The first impression is that of the *bucket-like* shape of the void, be it interspersed by a rather pronounced density enhancement near its centre. This profile shape does confirm to the general trend of low-density regions to develop a near uniform interior density surrounded by sharply defined boundaries. Because initially emptier inner regions expand faster than the denser outer layers the matter distribution gets evened out while the inner layers catch up with the outer ones.

Void Velocity Field

The flow in and around the void is dominated by the outflow of matter from the void, culminating into the void's own expansion near the outer edge. The comparison with the top two frames demonstrates the strong relation with features in the particle distribution and the density field. Not only is it slightly elongated along the direction of the void's shape, but it is also sensitive to some prominent internal features of the void. Towards the "SE"

direction the flow appears to slow down near a ridge, near the centre the DTFE reconstruction identifies two expansion centres.

The void velocity field profile is intimately coupled to that of its density field. The linear velocity increase is a manifestation of its general expansion. The near constant velocity divergence within the void conforms to the *super-Hubble flow* expected for the near uniform interior density distribution. Because voids are emptier than the rest of the universe they will expand faster than the rest of the universe with a net velocity divergence equal to

$$\theta \;=\; \frac{\nabla \cdot \mathbf{v}}{H} \;=\; 3(\alpha - 1)\,, \tag{2}$$

$$\alpha \;=\; H_{\rm void}/H\,, \tag{3}$$

where α is defined to be the ratio of the super-Hubble expansion rate of the void and the Hubble expansion of the universe.

Expanding Voids and the Cosmos

Evidently, the highest expansion ratio is that for voids which are completely empty, ie. $\Delta_{\rm void} = -1$. The expansion ratio α for such voids may be inferred from Birkhoff's theorem, treating these voids as empty FRW universes whose expansion time is equal to the cosmic time. For a matter-dominated Universe with zero cosmological constant, the maximum expansion rate that a void may achieve is given by

$$\theta_{\rm max} \;=\; 1.5\;\Omega_m^{0.6}\,, \tag{4}$$

with Ω_m the cosmological mass density parameter. For empty voids in a Universe with a cosmological constant a similar expression holds, be it that the value of α will have to be numerically calculated from the corresponding equation. In general the dependence on Λ is only weak. Generic voids will not be entirely empty, their density deficit $|\Delta_{\rm void}| \approx 0.8-0.9$ (cf. eg. the linear density profile in Fig. 25). The expansion rate $\theta_{\rm void}$ for such a void follows from numerical evaluation of the expression

$$\theta_{\rm void} \;=\; \frac{3}{2}\,\frac{\Omega_m^{0.6} - \Omega_{m,\rm void}^{0.6}}{1 + \frac{1}{2}\Omega_{m,\rm void}^{0.6}}\,; \qquad \Omega_{m,\rm void} \;=\; \frac{\Omega_m(\Delta_{\rm void}+1)}{(1+\frac{1}{3}\theta)^2} \tag{5}$$

in which $\Omega_{m,\rm void}$ is the effective cosmic density parameter inside the void.

When assessing the statistics of the velocity field divergence, using appropriate tools, one may indeed find a sharp positive divergence cutoff marking the maximum expansion rate of void regions. On the basis of their tessellation based technique, an early velocity field oriented version of DTFE, Bernardeau and van de Weygaert [16] and Bernardeau et al. [17] demonstrated that potentially one may indeed infer information on $\Omega_{m,0}$ from the expansion of voids.

4.4 Void Sociology

Computer simulations of the gravitational evolution of voids in realistic cosmological environments do show a considerably more complex situation than that described by idealized spherical or ellipsoidal models (see Martel and Wassermann [111], Regős and Geller [145], Dubinski et al. [53], van de Weygaert and van Kampen [187], Goldberg and Vogeley [68], Colberg et al. [36], Padilla et al. [125]). In recent years the huge increase in computational resources has enabled N-body simulations to resolve in detail the intricate substructure of voids within the context of hierarchical cosmological structure formation scenarios [7, 36, 68, 71, 78, 116, 125]. They confirm the theoretical expectation of voids having a rich substructure as a result of their hierarchical buildup (see e.g. Fig. 21).

Sheth and van de Weygaert [168] treated the emergence and evolution of voids within the context of *hierarchical* gravitational scenarios. It leads to a considerably modified view of the evolution of voids. The role of substructure within their interior and the interaction with their surroundings turn out to be essential aspects of the *hierarchical* evolution of the void population in the Universe. An important guideline are the heuristic void model simulations by Dubinski et al. [53], and the theoretical void study by Sahni et al. [156] within the context of a Lagrangian adhesion model approach by Sahni et al. [156]. Sheth and van de Weygaert [168] showed that the hierarchical development of voids, akin to the evolution of overdense halos, may be described by an *excursion set* formulation [22, 142, 167]. In some sense voids have a considerably more complex evolutionary path than overdense halos. This prodded the development of a two-barrier excursion set formalism (see Sect. 3.7 in accompanying lecture notes on the theory of the Cosmic Web). The two barriers refer to two processes that dictate the evolution of voids: their *merging* into ever larger voids as well as the *collapse* and disappearance of small ones embedded in overdense regions.

Void Merging

First, consider a small region which was less dense than the critical $\delta_{\rm v}$. It may be that this region is embedded in a significantly larger underdense region which is also less dense than the critical density. Many small primordial density troughs may exist within the larger void region. Once small voids located within the larger embedding underdensity have emerged as true voids at some earlier epoch, their expansion tends to slow down. Subsequently, they merge and get absorbed into the larger void emerging from the embedding underdensity as it reaches its shell-crossing phase. Therefore, we should identify the larger region as a large void today, while the smaller subvoids should not anymore be counted as such (see Fig. 26 bottom row).

Void Collapse

A *second* void process is responsible for the radical dissimilarity between void and halo populations. If a small scale minimum is embedded in a sufficiently high large scale density maximum, then the collapse of the larger surrounding region will eventually squeeze the underdense region it surrounds: the small-scale void will vanish when the region around it has collapsed completely. Alternatively, though usually coupled, they may collapse as a result of the tidal force field in which they find themselves. If the void within the contracting overdensity has been squeezed to vanishingly small size it should no longer be counted as a void (see Fig. 26 bottom row).

The collapse of small voids is an important aspect of the symmetry breaking between underdensities and overdensities. In the primorial Universe, Gaussian primordial conditions involve a perfect symmetry between

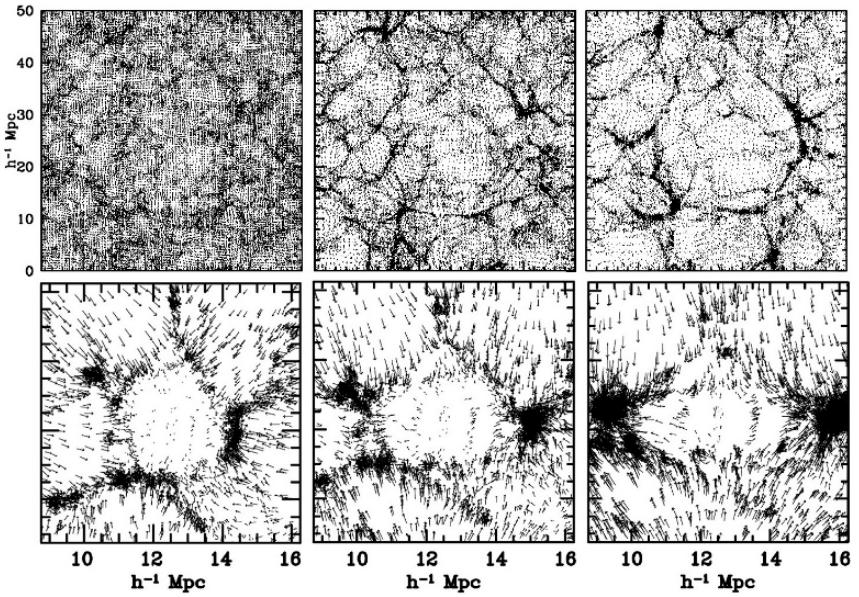

Fig. 26. The two modes of void evolution: void merging (**top row**) and void collapse (**bottom row**). **Top**: three timesteps of evolving void structure in a 128^3 particle N-body simulation of structure formation in an SCDM model ($a_{\rm exp} = 0.1, 0.3, 0.5$). The sequence shows the gradual development of a large void of diameter ≈ 25 h^{-1} Mpc as the complex pattern of smaller voids and structures which had emerged within it at an earlier time, merge with one another. It illustrates the *void-in-void* process of the evolving void hierarchy. **Bottom**: a choice of three collapsing voids in a constrained N-body simulation, each embedded within an environment of different tidal shear strength. The arrows indicate the velocity vectors, showing the infall of outer regions onto the void region. As a result the voids will be crushed as the surrounding matter rains down on them

under- and overdense. Any inspection of a galaxy redshift map or an N-body simulation shows that there is a marked difference between matter clumps and voids. While the number density of halos is dominated by small objects, void collapse is responsible for the lack of small voids.

4.5 Void Excursions

The excursion set formalism allows an elegant formulation and evaluation of the complex evolution of voids outlined above in terms of a *two-barrier* excursion set formalism. The *merging* and *collapse* barriers have been indicated by horizontal bars in the Brownian random walk diagram of Fig. 27. In the formalism developed by Sheth and van de Weygaert [168] the maturing/merging threshold is set to a fixed threshold value, independent of scale: the *shell-crossing* value $\delta_v = -2.81$ of spherical voids. The *void collapse* of an underdensity embedded within a contracting overdensity is set by the collapse barrier δ_c (for halos).

Void-in-Void and Void-in-Cloud

Since many small voids may coexist within one larger void, we must not count all of the smaller voids as distinct objects, lest we overestimate the

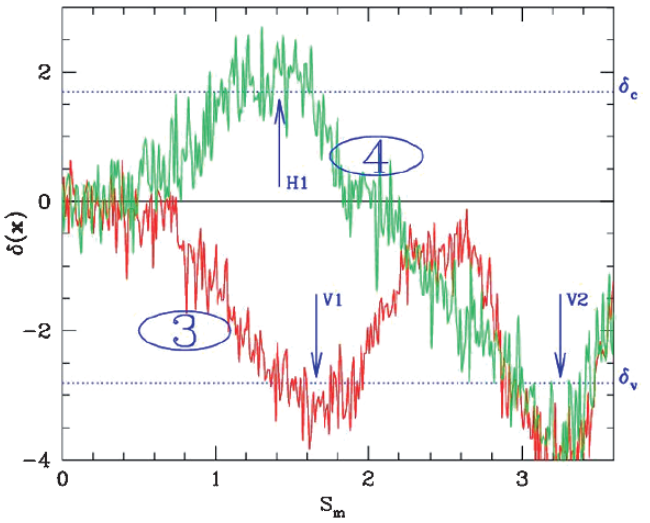

Fig. 27. Two-barrier excursion set formalism for the two void processes: void merging (red) and void collapse (green). Random walk exhibited by the average overdensity δ centred on a randomly chosen position in a Gaussian random field, as a function of smoothing scale, parametrized by S_M (large volume are on the left, small volumes on the right). Dashed horizontal lines indicate the collapse barrier δ_c and the void shell-crossing barrier δ_v

number of small voids and the total volume fraction in voids. This is called the *void-in-void* problem. In this case small voids from an early epoch merge with one another to form a larger void at a later epoch. It is analogous to the well-known *cloud-in-cloud* problem associated with the number density of initially overdense peaks. To account for the impact of voids disappearing when embedded in collapsing regions, we must also deal with the *void-in-cloud* problem. Also see Fig. 9 in van de Weygaert and Bond (2005).

By contrast, the evolution of overdensities is governed only by the *cloud-in-cloud* process; the *cloud-in-void* process is much less important, because clouds which condense in a large scale void are not torn apart as their parent void expands around them. This asymmetry between how the surrounding environment affects halo and void formation is incorporated into the *excursion set approach* by using one barrier to model halo formation and a second barrier to model void formation (Fig. 9 in van de Weygaert and Bond (2005)). Only the first barrier matters for halo formation, but both barriers play a role in determining the expected abundance of voids.

Brownian Void Walks

Figure 27 depicts two different random walks, each illustrative examples of the void evolution processes. The red Brownian random walk relates to the *void-in-void* trajectory of void formation through the merging of voids. The green Brownian random walk depicts the fateful events unfolding for a collapsing void, a *void-in-halo* trajectory. The *void-in-void* random walk looks very much the inverse of that for the cloud-in-cloud process associated with halo mergers. The associated random walk shows that the present-day void V1 contains more mass ($S \sim 1.6$) than the smaller void V2 ($S \sim 3.2$) which merged into $V1$. The red random walk concerns a location which at early times was found within a small void $V2$. This void, however, is embedded on a mass larger mass scale within an overdense halo $H1$. Once this entity collapses into a massive virialized halo, V2 will have disappeared.

If a walk first crosses $\delta_{\rm c}$ and then crosses $\delta_{\rm v}$ on a smaller scale, then the smaller void is contained within a larger collapsed region. Since the larger region has collapsed, the smaller void within it no longer exists, so it should not be counted. The only bona-fide voids are those associated with walks which cross $\delta_{\rm v}$ without first crossing $\delta_{\rm c}$. The problem of estimating the fraction of mass in voids reduces to estimating the fraction of random walks which first crossed $\delta_{\rm v}$ at S, and which did not cross $\delta_{\rm c}$ at any $S' < S$: the description of the void hierarchy requires solution of a *two-barrier* problem.

4.6 Void Spectrum

The analytical evaluation of the two-barrier random walk problem leads directly to a prediction of the distribution function $n_v(M)$ for voids on a mass

scale M. With respect to the linear extrapolated density field the matured void on a mass scale m corresponds to a fractional relative underdensity $\sqrt{\nu_v(M)}$,

$$\nu_v(M) \equiv \frac{|\delta_v|}{\sigma(M)}\,, \tag{6}$$

with the dependence on the mass scale M entering via the rms density fluctuation on that scale, $\sigma(M)$. According to the Sheth and van de Weygaert [168] the resulting void mass spectrum may be approximated by

$$n_v(M)\,\mathrm{d}M \approx \tag{7}$$
$$\sqrt{\frac{2}{\pi}}\,\frac{\rho_u}{M^2}\,\nu_v(M)\,\exp\left(-\frac{\nu_v(M)^2}{2}\right)\,\left|\frac{\mathrm{d}\ln\sigma(M)}{\mathrm{d}\ln M}\right|\,\exp\left\{-\frac{|\delta_{\rm v}|}{\delta_{\rm c}}\,\frac{\mathcal{D}^2}{4\nu_v^2}-2\frac{\mathcal{D}^4}{\nu_v^4}\right\}\,.$$

which for a pure power-law power spectrum yields

$$n_v(M)\,\mathrm{d}M \approx \sqrt{\frac{1}{2\pi}}\,\left(1+\frac{n}{3}\right)\,\frac{\rho_u}{M^2}\,\left(\frac{M}{M_{v,*}}\right)^{(3+n)/6}\,\exp\left\{-\left(\frac{M}{M_{v,*}}\right)^{(3+n)/3}\right\} \tag{8}$$
$$\times\,\exp\left\{-\frac{\mathcal{D}^2}{2}\,\left(\frac{|\delta_{\rm v}|}{4\delta_{\rm c}}+\mathcal{D}^2\left(\frac{M}{M_{v,*}}\right)^{-(3+n)/3}\right)\,\left(\frac{M}{M_{v,*}}\right)^{-(3+n)/3}\right\}\,.$$

The quantity $\mathcal{D}$ is the "*void-and-cloud parameter*",

$$\mathcal{D} \equiv \frac{|\delta_{\rm v}|}{(\delta_{\rm c}+|\delta_{\rm v}|)}\,. \tag{9}$$

It parameterizes the impact of halo evolution on the evolving population of voids: the likelihood of smaller voids being crushed through the *void-in-cloud* process decreases as the relative value of the collapse barrier $\delta_{\rm c}$ with respect to the void barrier $\delta_{\rm v}$ becomes larger.

Along with the derived void distribution a variety of related interesting observations may be made. One aspect concerns the fraction of mass contained in voids on mass scale M,

$$f(M) = \frac{M\,n_v(M)}{\rho_u}\,. \tag{10}$$

The resulting distribution is also peaked. The top lefthand frame of Fig. 28 shows that most of the void mass is indeed to be found in voids of characteristic mass $M_{v,*}$. At any given time the mass fraction in voids is approximately thirty percent of the mass in the Universe.

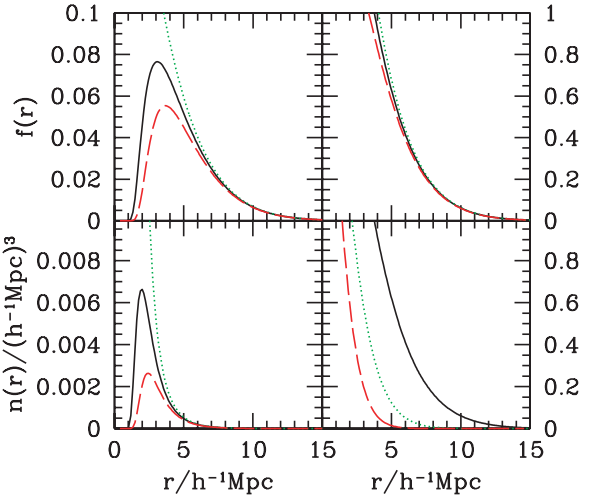

Fig. 28. Distribution of void radii predicted on the basis of (9), in an Einstein de-Sitter model with $P(k) \propto k^{-1.5}$, normalized to $\sigma_8 = 0.9$ at $z = 0$. Top left panel shows the mass fraction in voids of radius r. Bottom left panel shows the number density of voids of radius r. Note that the void-size distribution is well peaked about a characteristic size provided one accounts for the void-in-cloud process. Top right panel shows the cumulative distribution of the void volume fraction. Dashed and solid curves in the top panels and bottom left panel show the two natural choices for the importance of the void-in-cloud process discussed in the text: $\delta_c = 1.06$ and 1.686, with $\delta_v = -2.81$. Dotted curve shows the result of ignoring the *void-in-cloud* process entirely. Clearly, the number of small voids decreases as the ratio of $\delta_c/|\delta_v|$ decreases. Bottom right panel shows the evolution of the cumulative void volume fraction distribution. The three curves in this panel are for $\delta_c = 1.686(1+z)$, where $z = 0$ (*solid*), 0.5 (*dotted*) and 1 (*dashed*)

Characteristic Void Size

Expression (9) shows clearly that $n(M)$ cuts-off sharply at both small and large values of ν_v. This becomes clear when inspecting The number density $n_v(R)$ of voids of radius R[3] in Fig. 28 (bottom lefthand frame). It shows that the distribution of void masses is reasonably well peaked about $\nu \approx 1$, corresponding to a characteristic mass scale of order $\sigma_0(M) \approx |\delta_v|$.

The above implies that at any one cosmic epoch there is a *characteristic void size* which increases with time: the larger voids present at late time formed from mergers of smaller voids which formed at earlier times. For pure

[3] The conversion of the void mass scale to equivalent void radius R is done by assuming the simplest approximation, that of the spherical tophat model. According to this model a void has expanded by a factor of 1.7 by the time it has mature, so that $V_v = (M/\rho_u) * 1.7^3$.

power-law power spectra this means that this *self-similar* evolution of the void population centers around the evolving void mass $M_{v,*}$:

$$M_{v,*}(t) \propto D(t)^{6/(3+n)} M_{v,*,o}\,, \tag{11}$$

in which the present-day characteristic void mass, inversely proportional to $|\delta_v|$, is

$$M_{v,*,o} = \left(\frac{2A}{\delta_v^2}\right)^{3/(3+n)} . \tag{12}$$

Self-similar Void Evolution

In an Einstein de-Sitter universe, $\delta_{\rm c}$, $\delta_{\rm v}$ and $\sigma(m)$ all have the same time dependence, so (9) evolves self-similarly, parameterized by the characteristic *"void mass"* $M_{v,*}$. Also for more general world-models the approximation of self-similar void evolution should be quite accurate as the time dependences are only slightly different.

4.7 Void Evolution

The population of large voids is insensitive to the *void-in-cloud* process. The large mass cutoff of the void spectrum is similar to the ones for clusters and reflects the Gaussian nature of the fluctuation field from which the objects have condensed. The gradual merging of voids into ever larger ones is embodied in the self-similar shift of the peak of the void spectrum, ie. of $M_{v,*}$. The abundance of voids which larger than the typical initial comoving sizes of clusters is therefore reasonably described by peaks theory [10, 168].

While the two-barrier excursion set formalism offers an attractive theoretical explanation for the distinct asymmetry between clumps and voids and for the peaked void size distribution, we need to identify where the disappearing small-scale voids are to be found in a genuine evolving cosmic matter distribution. Using the GIF N-body simulations of various CDM scenarios, Platen [134] has managed to trace various specimen of this unfortunate void population. Using the new *Watershed Void Finder* technique [135] identified small-scale voids at high redshift ($z = 3$) and subsequently followed their evolution. Figure 29 shows the void distribution in and around a large central underdensity at four cosmic epochs, $z = 3.0, 2.0, 1.5$ and 0.5. The fate of the subvoids within the large present-day void is clearly visible: the interior ones tend to merge with surrounding peers while the ones near the boundary get squeezed out of existence. Close inspection shows that the small voids are not collapsing isotropically. Instead they tend to get sheared by their surroundings.

This image of void formation in the dark matter distribution has been elaborated by Furlanetto and Piran [64] to describe the implications for voids

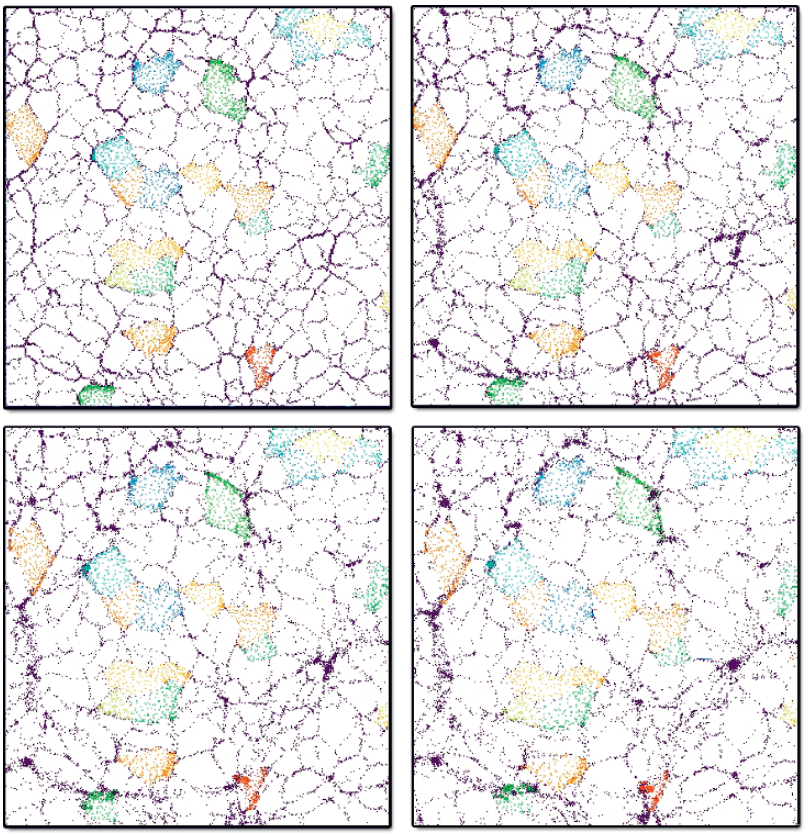

Fig. 29. Evolving Void Hierarchy: the structure in and around a large central void in a GIF ΛCDM simulation. At $z = 3$ the watershed WVF voidfinder [135] has been applied to trace the outline of voids in the matter distribution. Particles at the surrounding ridges (boundaries) are subsequently followed. The four frames depict the resulting particle distribution in a 5 h^{-1} Mpc thick and ≈ 60 h^{-1} Mpc wide slice, at 4 successive time intervals: $z = 3.0, 2.0, 1.5$ and 0.5. Clearly visible is the fate of subvoids within the large present-day void: either they merge into the background or they get squeezed out of existence near the boundary. From Platen et al. [136]. Courtesy GIF simulation: J. Colberg and Virgo consortium

in the galaxy distribution while it forms the starting point for various ongoing investigations.

The demise of small voids near the boundaries of large voids, touching the surrounding filaments and sheets, is a clear indication for the importance of tidal influences on the developing subvoid. Tidal stresses induced by the large scale vicinity will be of major importance for their final fate. One may argue that tidal influences are more important for voids than they are for halos. Because their underdensity is naturally limited ($\delta \geq -1$) and because their

size is expanding the environment retains a dominant dynamical influence, in particular over the outer region of the voids. The accompanying force field will in general be anisotropic and if strong enough enforce a shearing collapse. It is entirely in line with the recent observation by Park and Lee [127] and Platen, van de Weygaert and Jones [136], that the shape of voids is significantly affected by the tidal influence of the surrounding matter distribution.

4.8 Soapsud of Voids

An important aspect of the implied void population is that it is approximately *space-filling*. It underlines the adagio that the large scale distribution of matter may be compared to a *soapsud of expanding bubbles*. This follows from evaluation of the cumulative integral

$$f_V(M) \equiv \int_M^\infty (1.7)^3 \, \frac{M' \, n_v(M')}{\rho_u} \, \mathrm{d}M' \; . \tag{13}$$

where the factor 1.7 is an estimate of the excess expansion of the void based upon the spherical model for void evolution (see footnote). The resulting (current) cumulative void volume distribution is shown in the top righthand panel of Fig. 28. For a finite value of void radius R the whole of space indeed appears to be occupied by voids. Even more impressive is the corresponding self-similar evolution of the culumative void volume distribution $f_V(M, t)$. The bottom righthand frame of Fig. 28 shows the gradual shift of the cumulative volume distribution towards larger voids. The correct image appears to be that of a gradually unfolding bubbly universe in which the average size of the voids grows as small voids merge into ever larger ones.

5 Conclusion: Morphology of the Cosmic Web

The Megaparsec scale galaxy distribution defines one of the most intriguing spatial patterns in nature, the Cosmic Web. In these notes we have looked into the many diverse aspects of the available observational information. For a considerable period the spatial analysis of weblike structures has been based on rather ill-defined heuristic concepts, difficult to interpret within the context of existing theories. We have provided a review of the recent activity towards this direction. A set of techniques has opened the path towards a meaningful quantitative analysis. Morphologically, the most distinct elements of the Cosmic Web are filaments and voids. Filaments have figured prominently in the accompanying theoretical treatise van de Weygaert and Bond, 2005 on the formation of the web. In these lecture notes we have put special emphasis on the voids in cosmic matter and galaxy distribution.

6 Acknowledgments

We wish to thank Manolis Plionis and Omar López-Cruz for their invitation and the wonderful weeks in Mexico, and for their almost infinite patience regarding our shifting deadlines. RvdW is most grateful to the hospitality of the Canadian Institute for Astrophysics, where we commenced the project leading to these notes. Both authors thank Max-Planck-Institut für Astrophysik in Garching for providing the hospitality and facilities allowing the completion of these lecture notes. In particular we are indebted to Jacqueline van Gorkom, Hans Böhringer and George Rhee. Without their encouragement and the more than helpful assistance and understanding of Sonja Japenga of Springer Verlag we would not have managed to bring these notes to completion. To them we owe a major share of our gratitude ! RvdW is grateful to Miguel Aragón-Calvo for his permission to use and manipulate various figures from his Ph.D. thesis. He also acknowledges him and Erwin Platen for many inspiring discussions and their contributions towards obtaining insight into the evolution of the Cosmic Web. Most fondly we wish to thank Bernard Jones, for his enthusiastic and crucial support and inspiration, the many original ideas over the years and for his support in completing this manuscript hours past midnight ...

References

1. Abazajian, K., et al. (The SDSS collaboration): Astron. J. **126**, 2081 (2003)
2. Abell, G.: Astrophys. J. Suppl. **3**, 211 (1958)
3. Abell, G., Corwin, G.O., Olowin, R.P.: Astrophys. J. Suppl. **70**, 1 (1989)
4. Aikio, J., Mähönen, P.: Astrophys. J. **497**, 534 (1998)
5. Aragón-Calvo, M.A.: Morphology and dynamics of the Cosmic Web, Ph.D. thesis, Groningen University (2007)
6. Aragón-Calvo, M.A., Jones, B.J.T., van de Weygaert, R., van der Hulst, J.M.: Astron. Astrophys. **474**, 315 (2007)
7. Arbabi-Bidgoli, S., Müller, V.: Mon. Not. R. Astron. Soc. **332**, 205 (2002)
8. Babul, A., Starkman, G.D.: Astrophys. J. **401**, 28 (1992)
9. Bahcall, N.A.: Ann. Rev. Astron. Astrophys. **26**, 631 (1988)
10. Bardeen, J.M., Bond, J.R., Kaiser, N., Szalay, A.S.: Astrophys. J. **304**, 15 (1986)
11. Barrow, J.D., Bhavsar, S.P., Sonoda, D.H.: Mon. Not. R. Astron. Soc. **216**, 17 (1985)
12. Basilakos, S., Plionis, M., Rowan-Robinson, M.: Mon. Not. R. Astron. Soc. **323**, 47 (2001)
13. Basilakos, S., Plionis, M.: Astrophys. J. **550**, 522 (2001)
14. Benson, A.J., Hoyle, F., Fernando, T, Vogeley, M.S.: Mon. Not. Roy. Astron. Soc. **340**, 160 (2003)
15. Berlind, A.A., Frieman, J., Weinberg, D.H., Blanton, M.R., Warren, M.S., Abazajian, K., Scranton, R., Hogg, D.W., Scoccimarro, R., Bahcall, N.A., Brinkmann, J., Gott, III J.R., Kleinman, S.J., Krzesinski, J., Lee, B.C.,

Miller, C.J., Nitta, A., Schneider, D.P., Tucker, D.L., Zehavi, I.: Astrophys. J. Suppl. **167**, 1 (2006)
16. Bernardeau, F., van de Weygaert, R.: Mon. Not. R. Astron. Soc. **279**, 693 (1996)
17. Bernardeau, F., van de Weygaert, R., Hivon, E., Bouchet, F.: Mon. Not. R. Astron. Soc. **290**, 566 (1997)
18. Bertschinger, E.: Astrophys. J. **295**, 1 (1985)
19. Bertschinger, E., Dekel A, Faber, S.M., Dressler, A., Burstein, D.: Astrophys. J. **364**, 370 (1990)
20. Blumenthal, G.R., Da Costa, L., Goldwirth, D.S., Lecar, M., Piran, T.: Astrophys. J. **388**, 324 (1992)
21. Böhringer, H., Schuecker, P., Guzzo, L., Collins, C., Voges, W., Schindler, S., Neumann, D.M., Cruddace, R.G., DeGrandi, S., Chincarini, G., Edge, A.C., MacGillivray, H.T., Shaver, P.: Astron. Astrophys. **369**, 826 (2001)
22. Bond, J.R., Cole, S., Efstathiou, G., Kaiser, N.: Astrophys. J. **379**, 440 (1991)
23. Borgani, S., Guzzo, L.: Nature **409**, 39 (2001)
24. Bothun, G.D., Geller, M.J., Kurtz, M.J., Huchra, J.P., Schild, R.E.: Astrophys. J. **395**, 347 (1992)
25. Branchini, E., Teodoro, L., Frenk, C.S., Schmoldt, I., Efstathiou, G., White, S.D.M., Saunders, W., Sutherland, W., Rowan-Robinson, M., Keeble, O., Tadros, H., Maddox, S., Oliver, S.: Mon. Not. R. Astron. Soc. **308**, 1 (1999)
26. Branchini, E., Freudling, W., Da Costa, L.N., Frenk, C.S., Giovanelli, R., Haynes, M.P., Salzer, J.J., Wegner, G., Zehavi, I.: Mon. Not. R. Astron. Soc. **326**, 1191 (2001)
27. Braun, J., Sambridge, M.: Nature **376**, 655 (1995)
28. Carlstrom, J.E., Holder, G.P., Reese, E.D.: Ann. Rev. Astron. Astrophys. **40**, 643 (2002)
29. Ceccarelli, L., Padilla, N.D., Valotto, C., Lambas, D.G: Mon. Not. Roy. Astron. Soc. **373**, 1440 (2006)
30. Cen R., Miralda-Escudé J., Ostriker J.P., Rauch M.: Astrophys. J. **437**, 9 (1994)
31. Cen R., Ostriker J.: Astrophys. J. **650**, 560 (2006)
32. Chiang, L.-Y., Coles, P.: Mon. Not. R. Astron. Soc. **311**, 809 (2000)
33. Chincarini, G., Rood, H.J.: Nature **257**, 294 (1975)
34. Colberg, J.M.: Mon. Not. R. Astron. Soc. **375**, 337 (2007)
35. Colberg, J.M., Krughoff, K.S., Connolly, A.J.: Mon. Not. R. Astron. Soc. **359**, 272 (2005)
36. Colberg, J.M., Sheth, R.K., Diaferio, A., Gao, L., Yoshida, N.: Mon. Not. R. Astron. Soc. **360**, 216 (2005)
37. Colberg, J.M., Pearce, F., Foster, C., Platen, E., Brunino, R., Basilakos, S., Fairall, A., Feldman, H., Gottlöber, S., Hahn, O., Hoyle, F., Müller, V., Nelson, L., Neyrinck, M., Plionis, M., Porciani, C., Shandarin, S., Vogeley, M., van de Weygaert, R.: Mon. Not. R. Astron. Soc., subm. (2008)
38. Coles, P., Chiang, L.-Y.: Nature **406**, 376 (2000)
39. Colless, M., et al.: Astro-ph/0306581 (2003)
40. Colombi, S., Pogosyan, D., Souradeep, T.: Phys. Rev. Let. **85**, 5515 (2000)
41. Cressie, N.: Statistics for Spatial Data, rev. edn. John Wiley & Sons, Chichester (1993)
42. Davé R., et al.: Astrophys. J. **552**, 473 (2001)

43. Davis, M., Huchra, J., Latham, D.W., Tonry, J.: Astrophys. J. **253**, 423 (1982)
44. de Lapparent, V., Geller, M.J., Huchra, J.P.: Astrophys. J. **369**, 273 (1991)
45. de Lapparent, V., Geller, M.J., Huchra, J.P.: Astrophys. J. **302**, L1 (1986)
46. Dekel, A., Bertschinger, E., Faber, S.M.: Astrophys. J. **364**, 349 (1990)
47. Dekel, A.: Ann. Rev. Astron. Astrophys. **32**, 371 (1994)
48. Dekel, A., Lahav, O.: Astrophys. J. **520**, 24 (1999)
49. Dekel, A., Rees, M.J.: Nature **326**, 455 (1987)
50. Dekel, A., Rees, M.J.: Astrophys. J. **433**, L1 (1994)
51. Delaunay, B. N.: Bull. Acad. Sci. USSR Clase. Sci. Mat. **7**, 793 (1934)
52. Doré, O., Colombi, S., Bouchet, F.R.: Mon. Not. R. Astron. Soc. **344**, 905 (2003)
53. Dubinski, J., da Costa, L.N., Goldwirth, D.S., Lecar, M., Piran, T.: Astrophys. J. **410**, 458 (1993)
54. Ebeling, H., Edge, A.C., Allen, S.W., Crawford, C.S., Fabian, A.C.: Mon. Not. Roy. Astron. Soc. **318**, 333 (2000)
55. Einasto, J., Joeveer, M., Saar E.: Nature, **283**, 47 (1980)
56. El-Ad, H., Piran, T., da Costa, L.N.: Astrophys. J. **462**, L13 (1996)
57. El-Ad, H., Piran, T.: Astrophys. J. **491**, 421 (1997)
58. Erdoğdu, P., Lahav, O., Zaroubi, S., Efsathiou, G., Moody, S., Peacock, J.A., Colless, M., Baldry, I.K., Baugh, C.M., Bland-Hawthorn, J., 2dFGRS Team: Mon. Not. Roy. Astron. Soc. **352**, 939 (2004)
59. Erdoğdu, P., Huchra, J.P., Lahav, O., Colless, M., Cutri, R.M., Falco, E., George, T., Jarrett, T., Jones, D.H., Kochanek, C.S., Macri, L., Mader, J., Martimbeau, N., Pahre, M., Parker, Q., Rassat, A., Saunders, W.: Mon. Not. Roy. Astron. Soc. **368**, 1515 (2006)
60. Finoguenov A., Briel U.G., Henry J.P.: Astron. Astrophys. **410**, 777 (2003)
61. Fliche, H.H., Triay, R.: gr-qc/0607090 (2006)
62. Fukugita M., Hogan C., Peebles P.J.E.: Astrophys. J. **503**, 518 (1998)
63. Fukugita, M., Peebles, P.J.E.: Astrophys. J. **616**, 643 (2004)
64. Furlanetto, S.R., Piran, T.: Mon. Not. Roy. Astron. Soc. **366**, 467 (2006)
65. Gaztañaga, E.: Astrophys. J. **398**, L17 (1992)
66. Geller, M., Huchra, J. P.: Nature **246**, 897 (1989)
67. Gladders, M.D., Yee, H.K.C.: Astron. J. **120**, 2148 (2000)
68. Goldberg, D.M., Vogeley, M.S.: Astrophys. J. **605**, 1 (2004)
69. Gott, J.R. III, Dickinson, M., Melott, A.L.: Astrophys. J. **306**, 341 (1986)
70. Gott, J.R. III, Jurić, M., Schlegel, D., Hoyle, F., Vogeley, M., Tegmark, M., Bahcall, N., Brinkmann, J.: Astrophys. J. **624**, 463 (2005)
71. Gottlöber, S., Łokas, E.L., Klypin, A., Hoffman, Y.: Mon. Not. Roy. Astron. Soc. **344**, 715 (2003)
72. Graham, M.J., Clowes, R.G.: Mon. Not. R. Astron. Soc. **275**, 790 (1995)
73. Gregory, S.A., Thompson, L.A.: Astrophys. J. **222**, 784 (1978)
74. Grogin, N.A., Geller, M.J.: Astron. J. **118**, 256 (1999)
75. Grogin, N.A., Geller, M.J.: Astron. J. **119**, 32 (2000)
76. Hahn, O., Porciani, C., Carollo, M., Dekel, A.: Mon. Not. R. Astron. Soc. **375**, 489 (2007)
77. Heath Jones, D. et al.: Mon. Not. R. Astron. Soc. **355**, 747 (2004)
78. Hoeft, M., Yepes, G., Gottlöber, S., Springel, W.: Mon. Not. Roy. Astron. Soc. **371**, 401 (2006)
79. Hoffman, Y., Shaham, J.: Astrophys. J. **262**, L23 (1982)

80. Hoffman, Y., Silk, J., Wyse, R.F.G.: Astrophys. J. **388**, L13 (1992)
81. Hoyle, F., Vogeley, M.: Astrophys. J. **566**, 641 (2002)
82. Hoyle, F., Vogeley, M.: Astrophys. J. **580**, 663 (2002)
83. Huchra, J., et al. *Nearby large-scale structures and the zone of avoidance*, ASP Conf. Ser. Vol. 239, Fairall, K.P., Woudt, P.A., (Astron. Soc. Pac., San Francisco), p. 135 (2005)
84. Icke, V.: Mon. Not. R. Astron. Soc. **206**, 1P (1984)
85. Jones, B.J.T., Martínez, V.J., Saar, E., Trimble, V.: Rev. Mod. Phys. **76**, 1211 (2005)
86. Kaastra J.S., Lieu R., Tamura T., Paerels F.B.S., den Herder J.W.: Astron. Astrophys. **397**, 445 (2003)
87. Kaiser, N.: Astrophys. J. **284**, 9 (1984)
88. Kaiser, N.: Statistics of gravitational lensing 2: weak lenses. In: Martinez, V.J., Portilla, M., Saez, D. (eds.) New Insights into the Universe, Lecture Notes in Physics 408, p. 279. Springer-Verlag Berlin, Heidelberg, New York (1992)
89. Kaiser, N., Squires, G.: Astrophys. J. **404**, 441 (1993)
90. Kang H., Ryu D., Cen R., Song D.: Astrophys. J. **620**, 21 (2005)
91. Karachentseva, V.E., Karachentsev, I.D., Richter, G.M.: Astron. Astrophys. **135**, 221 (1999)
92. Karachentsev, I.D., Karachentseva, V.E., Huchtmeier, W.K., Makarov, D.I.: Astron. J. **127**, 2031 (2004)
93. Kauffmann, G., Fairall, A.P.: Mon. Not. R. Astron. Soc. **248**, 313 (1991)
94. Kauffmann, G., Colberg, J.M., Diaferio, A., White, S.D.M.: Mon. Not. R. Astron. Soc. **303**, 188 (1999)
95. Kim, R. S. J., Kepner, J.V., Postman, M., Strauss, M.A., Bahcall, N.A., Gunn, J.E., Lupton, R.H., Annis, J., Nichol, R.C., Castander, F.J., Brinkmann, J., Brunner, R.J., Connolly, A., Csabai, I., Hindsley, R.B., Izević, Ž., Vogeley, M.S., York, D.G.: Astron. J. **123**, 20 (2002)
96. Kirshner, R.P., Oemler, A., Schechter, P.L., Shectman, S.A.: Astrophys. J. **248**, L57 (1981)
97. Kirshner, R.P., Oemler, A., Schechter, P.L., Shectman, S.A.: Astrophys. J. **314**, 493 (1987)
98. Kitaura, F.S., Enßlin, T.A.: arXiv:0705.0429 (2007)
99. Kocevski, D.D., Ebeling, H.: Astrophys. J. **645**, 1043 (2006)
100. Kochanek, C.S., White, M., Huchra, J., Macri, L., Jarrett, T.H., Schneider, S.E., Mader, J.: Astrophys. J. **585**, 161 (2003)
101. Kuhn, B., Hopp, U., Elsässer, H.: Astron. Astrophys. **318**, 405 (1997)
102. Lachieze-Rey, M., da Costa, L.N., Maurogordata, S.: Astrophys. J. **399**, 10 (1992)
103. Lee, J., Park, D.: Phys. Rev. Lett (subm), arXiv0704.0881L (2007)
104. Lieu, R., Mittaz, J.P.D., Zhang, S.-N.: Astrophys. J. **648**, 176 (2006)
105. Little, B., Weinberg, D.H.: Mon. Not. Roy. Astron. Soc. **267**, 605 (1994)
106. Lombardi, M., Schneider P.: Astron. Astrophys. **373**, 359 (2001)
107. Lombardi, M., Schneider P.: Astron. Astrophys. **392**, 1153 (2002)
108. Lombardi, M., Schneider P.: Astron. Astrophys. **407**, 385 (2003)
109. López-Cruz, O.: Photometric properties of low-redshift galaxy clusters. Ph.D. thesis, Univ. Toronto (1997)
110. Luo, R., Vishniac, E.: Astrophys. J. Suppl. **96**, 429 (1995)
111. Martel, H., Wasserman, I.: Astrophys. J. **348**, 1 (1990)

112. Martínez, V., Saar E.: Statistics of the Galaxy Distribution, Chapman & Hall/CRC Press, USA (2002)
113. Martínez, V., Starck, J.-L., Saar, E., Donoho, D.L., Reynolds, S.C., de la Cruz, P., Paredes, S.: Astrophys. J. **634**, 744 (2005)
114. Massey, R., Rhodes, J., Ellis, R., Scoville, N., Leauthaud, A., Finoguenov, A., Capak, P., Bacon, D., Aussel, H., Kneib, J.-P., Koekemoer, A., McCracken, H., Mobasher, B., Pires, S., Refregier, A., Sasaki, S., Starck, J.-L., Taniguchi, Y., Taylor, A., Taylor, J.: Nature **445**, 286 (2007)
115. Matarrese, S., Coles, P., Lucchin, F., Moscardini, L.: Mon. Not. Roy. Astron. Soc. **286**, 115 (1997)
116. Mathis, H., White, S.D.M.: Mon. Not. Roy. Astron. Soc. **337**, 1193 (2002)
117. Mecke, K.R., Buchert, T., Wagner, H.: Astron. Astrophys. **288**, 697 (1994)
118. Mellier, Y.: Ann. Rev. Astron. Astrophys. **37**, 127 (1999)
119. Miller, C.J., Nichol, R.C., Reichart, D., Wechsler, R.H., Evrard, A.E., Annis, J., McKay, T.A., Bahcall, N.A., Bernardi, M., Böhringer, H., Connolly, A.J., Goto, T., Kniazev, A., Lamb, D., Postman, M., Schneider, D.P., Sheth, R.K., Voges, W.: Astron. J. **130**, 968 (2005)
120. Mo, H.J., White, S.D.M.: Mon. Not. Roy. Astron. Soc. **282**, 347 (1996)
121. Nicastro K., et al.: Nature **421**, 719 (2003)
122. Novikov, D., Colombi, S., Doré, O.: Mon. Not. R. Astron. Soc. **366**, 1201 (2006)
123. Okabe, A., Boots, B., Sugihara, K., Chiu, S. N.: Spatial Tessellations : Concepts and Applications of Voronoi Diagrams, 2nd ed. John Wiley & Sons, Chichester, Toronto (2000)
124. Oort, J.H.: Ann. Rev. Astron. Astrophys. **21**, 373 (1983)
125. Padilla, N.D., Ceccarelli, L., Lambas, D.G.: Mon. Not. Roy. Astron. Soc. **363**, 977 (2005)
126. Palmer, P.L, Voglis, N.: Mon. Not. R. Astron. Soc. **205**, 543 (1983)
127. Park, D., Lee, J.: Phys. Rev. Lett. **98**, 081301 (2007)
128. Patiri, S.G., Betancort-Rijo, J.E., Prada, F., Klypin, A., Gottlöber, S.: Mon. Not. R. Astron. Soc. **369**, 335 (2006)
129. Patiri, S.G., Prada, F., Holtzman, J., Klypin, A., Betancort-Rijo, J.E.: Mon. Not. R. Astron. Soc. **372**, 1710 (2006)
130. Peebles, P.J.E.: The Large-Scale Structure of the Universe, Princeton University Press (1980)
131. Peebles, P.J.E.: Astrophys. J. **557**, 495 (2001)
132. Pichon C., Vergely J.L., Rollinde E., Colombi S., Petitjean P.: Mon. Not. R. Astron. Soc. **326**, 597 (2001)
133. Pimbblet, K.A.: Mon. Not. R. Astron. Soc. **358**, 256 (2005)
134. Platen, E.: Segmenting the Universe. M.Sc. thesis, Groningen University (2005)
135. Platen, E., van de Weygaert, R., Jones, B.J.T.: Mon. Not. R. Astron. Soc. **380**, 551 (2007)
136. Platen, E., van de Weygaert, R., Jones, B.J.T.: Mon. Not. R. Astron. Soc., subm, arXiv:0711.2480 (2008)
137. Plionis, M., Valdarnini, R.: Mon. Not. R. Astron. Soc. **249**, 46 (1991)
138. Plionis, M., Kolokotronis, V.: Astrophys. J. **500**, 1 (1998)
139. Plionis, M., Basilakos, S.: Mon. Not. R. Astron. Soc. **330**, 399 (2002)
140. Popescu, C.C., Hopp, U., Elsässer, H.: Astron. Astrophys. **325**, 881 (1997)
141. Popessu, P., Böhringer, H., Brinkmann, J., Voges, W., York, D.G.: Astron. Astrophys. **423**, 449 (2004)

142. Press, W.H., Schechter, P.: Astrophys. J. **187**, 425
143. Rauch M.: Ann. Rev. Astron. Astrophys. **36**, 267 (1998)
144. Refregier, Y.: Ann. Rev. Astron. Astrophys. **41**, 645 (2003)
145. Regős, E., Geller, M.J.: Astrophys. J. **373**, 14 (1991)
146. Reiprich, T.H., Böhringer, H.: Astron. Nachr. **320**, 296 (1999)
147. Ripley, B.D.: Spatial Statistics, Wiley & Sons, Chichester 1981 (1981)
148. Rojas, R.R., Vogeley, M.S., Hoyle, F., Brinkmann, J.: Astrophys. J. **624**, 571 (2005)
149. Romano-Díaz, E., van de Weygaert, R: Mon. Not. Roy. Astron. Soc. **382**, 2 (2007)
150. Rozo E, Wechsler, R.H.. Koester, B.P., McKay, T.A., Evrard, A.E., Johnston, D., Sheldon, E.S., Annis, J., Frieman, J.A.: arXiv:astro-ph/0703571 (2007)
151. Rudnick, L., Brown, S., Williams, L.R.: Astrophys. J. **671**, 40 (2007)
152. Rybicki, G.B., Press, W.H.: Astrophys. J. **398**, 169 (1992)
153. Ryden, B.S., Gramann, M.: Astrophys. J. **383**, 33 (1991)
154. Ryden, B.S., Melott, A.L.: Astrophys. J. **470**, 160 (1996)
155. Saar, E., Martiínez, V.J., Starck, J.-L., Donoho, D.L.: Mon. Not. Roy. Astron. Soc. **374**, 1030 (2007)
156. Sahni, V., Sathyaprakash, B.S., Shandarin, S.F.: Astrophys. J. **431**, 20 (1994)
157. Sahni, V., Shandarin, S.F.: Mon. Not. R. Astron. Soc. **282**, 641 (1996)
158. Sahni, V., Sathyaprakash, B.S., Shandarin, S.F.: Astrophys. J. **495**, 5 (1998)
159. Scaramella, R., Vettolani, G., Zamorani, G.: Astrophys. J. **376**, L1 (1991)
160. Schaap, W. E.: The delaunay tessellation field estimator. Ph.D. thesis, Groningen University (2007)
161. Schaap, W. E., van de Weygaert, R.: Astron. Astrophys. **363**, L29 (2000)
162. Schmalzing, J., Buchert, T., Melott, A.L., Sahni, V., Sathyaprakash, B.S., Shandarin, S.F.: Astrophys. J. **526**, 568 (1999)
163. Schmidt, J.D., Ryden, B.S., Melott, A.L.: Astrophys. J. **546**, 609 (2001)
164. Shandarin, S.F., Sheth, J.V., Sahni, V.: Mon. Not. R. Astron. Soc. **353**, 162 (2004)
165. Shandarin, S., Feldman, H.A., Heitmann, K., Habib, S.: Mon. Not. R. Astron. Soc. **376**, 1629 (2006)
166. Shectman, S.A., Landy, S.D., Oemler, A., Tucker, D.L., Lin, H., Kirshner, R.P., Schechter, P.L.: Astrophys. J. **470**, 172 (1996)
167. Sheth, R.K.: Mon. Not. R. Astron. Soc. **300**, 1057 (1998)
168. Sheth, R. K., van de Weygaert, R.: Mon. Not. R. Astron. Soc. **350**, 517 (2004)
169. Sibson, R.: Math. Proc. Cambridge Phil. Soc. **87**, 151 (1980)
170. Sibson, R.: A brief description of natural neighbor interpolation. In: *Interpreting Multi-variate Data*, ed. by V. Barnett (Wiley, Chichester 1981) pp. 21–36
171. Sousbie, T.: Le squelette de l'Univers: un nouvel outil d'analyse topologique des grandes structures. Ph.D. thesis l'Ecole Normale Supérieure de Lyon (2006)
172. Sousbie, T., Pichon, C., Colombi, S., Novikov, D., Pogosyan, D.: astroph/ 07073123 (2007)
173. Stoica, R.S., Martínez, V.J., Mateu, J., Saar, E.: Astron. Astrophys. **434**, 423 (2005)
174. Sukumar, N.: The natural element method in solid mechanics. Ph.D. thesis, Northwestern University (1998)
175. Sunyaev, R.A., Zel'dovich, Y.B.: Comments Astrophys. Space Phys. **2**, 66 (1970)

176. Sunyaev, R.A., Zel'dovich, Y.B.: Comments Astrophys. Space Phys. **4**, 173 (1972)
177. Szapudi, I.: Astrophys. J. **497**, 16 (1998)
178. Szomoru, A., van Gorkom, J.H., Gregg, M.D., Strauss, M.A.: Astron. J. **111**, 2150 (1996)
179. Tegmark, M., Peebles, P.J.E.: Astrophys. J. **500**, L79 (1998)
180. Tegmark, M., SDSS Collaboration: Astrophys. J. **606**, 702 (2004)
181. Tikhonov, A.V., Karachentsev, I.D.: Astrophys. J. **653**, 969 (2006)
182. Tikhonov, A.V., Klypin, A.: arXiv:0708.2348v1 (2007)
183. Tully, R.B.: Nearby Galaxy Catalog, Cambridge University Press, Cambridge, (1988)
184. Tully, R.B., Shaya, E.J., Karachentsev, I.D., Courtois, H., Kocevski, D.D., Rizzi, L., Peel, A.: arXiv:0705.4139v1 (2007)
185. Vale, C., White, M.: New Astronomy. **11**. 207 (2006)
186. van de Weygaert, R.: Voids and the geometry of large scale structure. Ph.D. thesis, Leiden University (1991)
187. van de Weygaert, R., van Kampen, E.: Mon. Not. R. Astron. Soc. **263**, 481 (1993)
188. van de Weygaert, R., Schaap, W.E: The Cosmic Web: geometric analysis. In: Mart nez, V., Saar, E., Mart nez-Gonzalez, E., Pons-Borderia, M. (eds.) Data Analysis in Cosmology, lectures summerschool Valencia 2004, p. 129. Springer-Verlag (2007)
189. van de Weygaert, R., Bond, J.R.: Clusters and the theory of the Cosmic Web. In: Plionis, M., López-Cruz, O., Hughes, D., (eds.) A Pan-Chromatic View of Clusters of Galaxies and the LSS, Springer (2008)
190. van Haarlem, M., van de Weygaert, R.: Astrophys. J. **418**, 544 (1993)
191. Voronoi, G.: J. Reine Angew. Math. **134**, 167 (1908)
192. Watson, D.F.: *Contouring: A guide to the analysis and display of spatial data*, Pergamom Press, Oxford (1992)
193. White, S.D.M.: Mon. Not. R. Astron. Soc. **186**, 145 (1979)
194. Willick, J.A., Courteau, S., Faber, S.M., Burstein, D., Dekel, A., Strauss, M.A.: Astrophys. J. Suppl. **109**, 333 (1997)
195. Wittman, D., Dell'Antonio, I.P, Hughes, J.P., Margoniner, V.E., Tyson, J.A., Cohen, J.G., Norman, D.: Astrophys. J. **643**, 128 (2006)
196. Yee, H.K.C., López-Cruz, O.: Astron. J. **117**, 1985 (1999)
197. Zel'dovich, Ya.B., Einasto, J., Shandarin, S.F.: Nature **300**, 407 (1982)